THESIS FOR THE DEGREE OF DOCTOR OF PHILOSOPHY

Partial Oxidation of Methane over Functionalised Zeolites and Zeotypes

XUETING WANG

CHALMERS

Department of Chemistry and Chemical Engineering
CHALMERS UNIVERSITY OF TECHNOLOGY
GOTHENBURG, SWEDEN 2018

Partial Oxidation of Methane over Functionalised Zeolites and Zeotypes
XUETING WANG

ISBN: 978-91-7597-817-8

Doktorsavhandlingar vid Chalmers tekniska högskola
Ny serie nr. 4498
ISSN 0346-718X

Department of Chemistry and Chemical Engineering
Chalmers University of Technology
SE-412 96 Gothenburg
Sweden
Telephone +46 31 772 1000

Cover:
Partial oxidation of methane (1) to methanol (2) through methoxy species at the Brønsted acid sites (3) and at the Cu dimer sites (4) in a Cu-zeolite sample (5, a transmission electron microscopy image of a Cu-ZSM-5 sample).

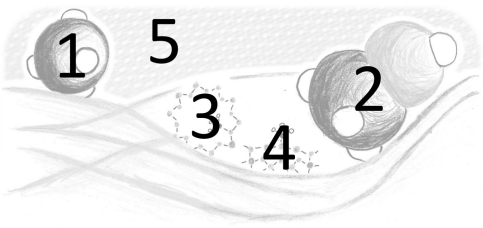

Typeset in LaTeX
Printed by Chalmers Digitaltryck
Gothenburg, Sweden 2018

Partial Oxidation of Methane over Functionalised Zeolites and Zeotypes
XUETING WANG
Department of Chemistry and Chemical Engineering
Chalmers University of Technology

Abstract

Partial oxidation of methane to methanol is an industrially important process that allows natural gas and biogas to be utilised for methanol-based production of chemicals or converted to liquid methanol fuel, which make transportation more facile. In this thesis, the activity for partial oxidation of methane to methanol over copper functionalised zeolites and silica supported copper is investigated using a three-step quasi-catalytic approach including catalyst activation, methane reaction and methanol extraction by water. Methanol is produced over isolated copper ions but likely not over copper particles. Under methane oxidation conditions, *in situ* infrared spectroscopy measurements show the formation of methoxy species adsorbed on the Brønsted acid sites, which is concluded to be an important reaction intermediate in the methanol formation.

The dynamic interaction between methanol and copper zeolites was experimentally studied by temperature-programmed desorption of methanol using a chemical flow reactor and *in situ* infrared spectroscopy and theoretically by first-principles calculations. It is shown that methoxy species binds strongly to the Brønsted acid sites in the zeolites, which explains the need for the extraction step as to obtain methanol from zeolite-based systems. The results indicate that methanol formation and desorption without using water extraction may require a catalyst with lower acidity.

The last part of this thesis investigates the possibility of tuning the catalyst acidity by synthesising so-called zeotypes to replace the zeolites. A boron silicate with chabazite structure and lower acidity compared to zeolitic chabazite was synthesised and functionalised with copper. Upon methane exposure to the copper boron silicate, methoxy species forms and retains on the copper sites, which is promising for methanol production. Further, three iron and/or aluminium containing silicates with MFI structure were synthesised. Through infrared spectroscopic surface analysis, it is shown that their acidity is lower than that of the corresponding zeolite structure, and thus these materials may be potential catalyst candidates that deserves further studies.

Keywords: Natural gas; Biogas; Green methanol; Heterogeneous catalysis; Temperature-programmed desorption; *In situ* infrared spectroscopy; FTIR; Zeolite; zeotype; Cu-ZSM-5; Cu-SSZ-13; Copper boron silicate.

List of Publications

This thesis is based on the following appended papers:

I. Copper Modified Zeolites and Silica for Conversion of Methane to Methanol
X. Wang, N. M. Martin, J. Nilsson, J. Gustafson, S. Carlson, M. Skoglundh and P.-A. Carlsson
Submitted for publication to Catalysts

II. Speciation of Gas Phase Products from Cu-zeolites during Temperature Programmed Desorption of Pre-adsorbed Methanol
X. Wang, A. A. Arvidsson, A. Hellman, M. Skoglundh, and P.-A. Carlsson
Manuscript

III. Methanol Desorption from Cu-ZSM-5 Studied by *In Situ* Infrared Spectroscopy and First-Principles Calculations
X. Wang, A. A. Arvidsson, M. O. Cichocka, X. Zou, N. M. Martin, J. Nilsson, S. Carlson, J. Gustafson, M. Skoglundh, A. Hellman and P.-A. Carlsson
Journal of Physical Chemistry C, 121 (**2017**), 27389-27398

IV. Methane Adsorption and Methanol Desorption of Copper Modified Boron Silicate
X. Wang, A. Shishkin, F. Hemmingsson, M. Skoglundh, F. J. Martinez-Casado, L. Bock, A. Idström, L. Nordstierna, H. Härelind and P.-A. Carlsson
RSC Advances, 8 (**2018**), 36369-36374

V. Tuned Acidity for Catalytic Reactions: Synthesis and Characterization of Fe- and Al-MFI Zeotypes
Simone Creci, X. Wang, P.-A. Carlsson and M. Skoglundh
Submitted for publication to Topics in Catalysis

Publications not included in the thesis:

Silver/Alumina for Methanol-Assisted Lean NO_x Reduction-On the Influence of silver Species and Hydrogen Formation
M. Männikkö, X. Wang, M. Skoglundh and H. Härelind
Applied Catalysis B: Environmental, 180 (**2016**), 291-300

Characterization of the Active Species in the Silver/Alumina System for Lean NO_x Reduction with Methanol
M. Männikkö, X. Wang, M. Skoglundh and H. Härelind
Catalysis Today, 267 (**2016**), 76-81

Characterization of Surface Structure and Oxidation/Reduction Behavior of Pd-Pt/Al_2O_3 Model Catalysts
N. M. Martin, J. Nilsson, M. Skoglundh, E. C. Adams, X. Wang, P. Velin, G. Smedler, A. Raj, D. Thompsett, H. H. Brongersma, T. Grehl, G. Agostini, O. Mathon, S. Carlson, K. Norén, F. J. Martinez-Casado, Z. Matej, O. Balmes and P.-A. Carlsson
Journal of Physical Chemistry C, 120 (**2016**), 28009-28020

Study of Methane Oxidation over Alumina Supported Pd-Pt Catalysts Using *operando* DRIFTS/MS and *in situ* XAS Techniques
N. M. Martin, J. Nilsson, M. Skoglundh, E. C. Adams, X. Wang, G. Smedler, A. Raj, D. Thompsett, G. Agostini, S. Carlson, K. Norén, and P.-A. Carlsson
Catalysis, Structure & Reactivity, 3 (**2017**), 24-32

Structure-function Relationship during CO_2 Methanation over Rh/Al_2O_3 and Rh/SiO_2 Catalysts at Atmospheric Pressure Conditions
N. M. Martin, F. Hemmingsson, X. Wang, L. R. Merte, U. Hejral, J. Gustafson, M. Skoglundh, D. Motta Meira, A.-C. Dippel, O. Gutowski, M. Bauer, and P.-A. Carlsson
Catalysis Science & Technology, 8 (**2018**), 2686–2696

My Contributions to the Publications

Paper I
I prepared all samples, planned and performed all experimental work and data analysis, interpreted the results together with my co-authors, and wrote the first draft of the manuscript.

Paper II
I prepared all samples, planed and performed all experimental work and data analysis, interpreted the results together with my co-authors, and wrote the first draft of the manuscript

Paper III
I prepared the catalysts, planned and performed all experimental work and data analysis except for the TEM measurements, interpreted the results together with my co-authors, and wrote the first draft of the manuscript

Paper IV
I prepared the Cu-BS sample, planned and performed all IR measurements, most of the calorimeter experiments and data analysis in the manuscript, interpreted the results together with my co-authors, and wrote the first draft of the manuscript.

Paper V
I participated in planning of the IR measurements and co-authored the manuscript.

Conference contributions

Influence of Ag Species and Surface Acidity on Methanol-SCR over Ag/Al_2O_3
X. Wang, M. Männikkö, M. Skoglundh and H. Härelind
Poster presentation at the 10th International Congrass on Catalysis and Automotive Pollution Control (CAPoC10)
28-30 August 2015, Brussels, Belgium

Characterization of Metal-Exchanged Zeolites for Direct Conversion of Methane to Methanol (DCMM)
X. Wang, M. Skoglundh, A. Hellman, J. Gustafson, and P.-A. Carlsson
Poster presentation at the 11th Natural Gas Conversion Symposium (NGCS 11)
05-09 June 2016, Tromsø, Norway

Dream Reaction Come True? Direct Conversion of Methane to Methanol over Cu-zeolites
X. Wang, A. A. Arvidsson, M. Skoglundh, A. Hellman, J. Gustafson, and P.-A. Carlsson
Oral presentation at the 13th European Congress on Catalysis (EUROPACAT 2017)
27-31 August 2017, Florence, Italy

Dream Reaction Come True? Direct Conversion of Methane to Methanol over Cu-zeolites
X. Wang, A. A. Arvidsson, M. Skoglundh, A. Hellman, J. Gustafson, and P.-A. Carlsson
Popular Science presentation at Material Science Graduate Student Days 2017
21 February 2017, Göteborg, Sweden

Dream Reaction Come True? Direct Conversion of Methane to Methanol over Cu-zeolite/zeotype
X. Wang, A. Shishkin, L. Nordstierna, H. Härelind, M. Skoglundh, and P.-A. Carlsson

A Local Gas-Sampling System for Quantitative Mass-Spectrometric Investigations of Chemical Reactions
A. Schaefer, X. Wang, F. Hemmingsson, P. Velin and P.-A. Carlsson
Poster presentations at Tailored Surfaces in Operando Conditions (TAILOR 2018)
11-14 June 2018, Ystad, Sweden

CONTENTS

CHAPTER 1

INTRODUCTION

1.1 Methane utilisation

Methane consists of one carbon and four hydrogen atoms and is chemically written as CH_4. It is the simplest molecule among the saturated hydrocarbons, which are called the alkanes. Methane is also the main component of natural gas that presently attracts much attention as, on the one hand, an abundant energy reserve[1] and, on the other hand, a source of carbon for production of chemicals[2]. Natural gas is a finite fossil resource and from the perspective of sustainable development its use should be minimised. Many industrial processes, however, driven by natural gas and/or designed for valorisation of natural gas can be made greener if biomethane is used instead. Figure 1.1 depicts a simplified carbon cycle for biomethane utilisation. Unlike conventional natural gas, biomethane is produced from biodegradable waste or renewable wood that restore carbon dioxide from the earth's atmosphere[3] upon growth. Thus, processes utilising biomethane may have a much lower or even zero carbon footprint.

Thanks to its low carbon-to-hydrogen ratio, methane delivers more useful energy per formed carbon dioxide upon combustion as compared to other hydrocarbon-based fuels[4]. Combustion is therefore one common process to utilise methane for power generation and vehicle propulsion. Though methane combustion has many advantages, slip of methane from the process to the atmosphere needs to be carefully controlled as methane is a strong greenhouse gas. Its global warming potential is 64 relative to CO_2 over a 20 years perspective[5]. Moreover, methane is used as a feedstock for producing chemicals through syngas (H_2 and CO), *e.g.*, ammonia, methanol, and liquids (fuels)[2]. In those processes, further improvements of chemical technologies for easy conversion of methane are still needed. Enabling technologies for efficient conversion of methane to chemicals would also be attractive for eliminating the gas flaring beside oil produc-

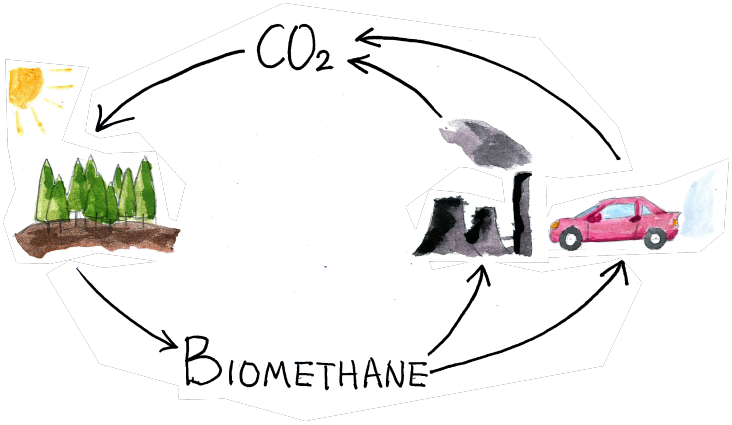

Figure 1.1: Simplified carbon cycle involving biomethane for two possible applications: chemical feedstock and vehicle fuel.

tion sites, where an equivalent of 5% of global production of natural gas is wasted due to lack of alternative solutions[6].

Regardless of the purpose, *e.g.* eliminating gas flaring or utilising biomethane for production of chemicals, it is attractive to convert the gaseous methane to a liquid product, for convenient transportation and storage at ambient conditions, and for usage at chemical plants. Methanol is one choice that presently attracts much interest[7,8] as it benefits all these aspects. Methanol as a target product is also environmentally sound as methanol is biodegradable. Present industrial conversion of methane to methanol is a two-step process where methane is first partially oxidised to syngas at high temperature and subsequently converted to methanol over a $Cu/ZnO/Al_2O_3$ catalyst at high pressure. The overall process, however, is energy intense and thus costly. In some cases it may also be atomically uneconomic due to total oxidation of methane to CO_2 and H_2O. Therefore, partial oxidation of methane to methanol at low temperature and ambient pressure is a desired atom economic alternative with potential low energy needs.

Catalysis is the phenomenological base for core chemical technologies for methane utilisation. Catalytic processes have been used by mankind long before the conception 'catalysis' was coined. Over the centuries, catalytic phenomena have been recognised in natural fermentation processes as well as used in key technologies for environmental protection[9] and greener energy conversion processes[10]. Catalysis has driven individual discoveries and stimulated systematic scientific research. The term catalysis was presented by the Swedish chemist Jöns Jacob Berzelius in 1835[11] although Elisabeth Fulhame touched upon the subject even earlier, in the late 1780s and early 1790s[12]. Catalysis is described as the phenomenon where the rate of a chemical reaction is affected by addition of a substance (the catalyst) in small quantity, and in which the substance is not consumed in large amount during the reaction. The main role of a catalyst is to provide an alternative path, often with lower activation barrier(s), for the

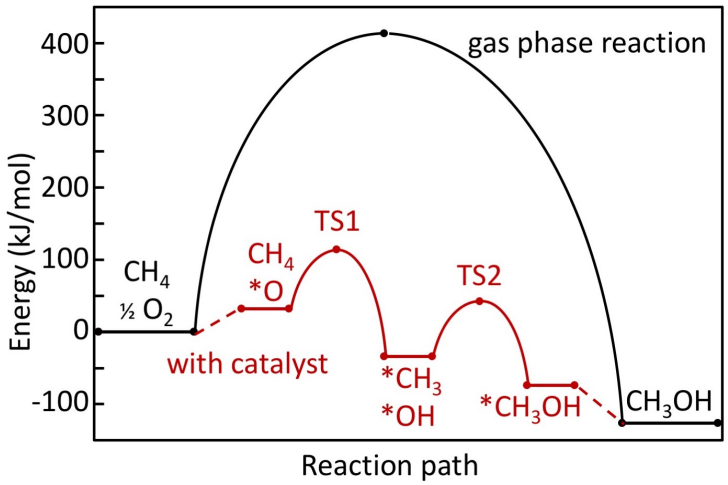

Figure 1.2: A simplified reaction energy diagram of partial oxidation of methane to methanol. The presence of the catalyst provides an alternative reaction pathway with lower activation energy than the gas phase reaction. The energy landscape of the gas phase reaction is simplified using the C-H bond activation energy as the barrier. The energy landscape of the catalytic route is adapted from a theoretical study of methane to methanol over Cu-ZSM-5 [13].

reaction to take place, as illustrated in Figure 1.2. Catalysed reactions are classified as either heterogeneous or homogeneous catalytic processes in which the catalyst is in different or the same physical phase as the reactants/products, respectively. Catalysis research includes a broad range of disciplines. The common goal among them is to improve the catalytic performance by understanding the catalyst material and the catalytic processes. The ultimate fascination is to study the catalyst while the catalytic process proceeds, *i.e.* under *operando* conditions, where it is possible to observe material characteristics, reaction intermediates and their evolution during the reaction as important ingredients of the catalytic action. With the development of advanced photon in-photon out characterisation methods, especially spectroscopic and scattering techniques, it is possible to capture a glimpse of material properties, down to the atomic level, that determine the catalytic cycle and the reaction rate.

1.2 Objectives

The objectives of the thesis is to evaluate copper containing zeolites and zeotypes as catalysts for partial oxidation of methane to methanol, investigate their dynamic interaction with methanol and understand how catalytic materials for partial oxidation of methane to methanol can be improved.

CHAPTER 2

PARTIAL OXIDATION OF METHANE TO METHANOL

Targeting a once-through industrial process for production of methanol from methane, high selectivity must be obtained by a controlled partial oxidation of methane in which unwanted further oxidation reactions are avoided. This is extremely challenging due to the fact that methane activation usually requires high energy inputs, *e.g.* in the form of heat, while formed methanol may easily decompose to other more thermodynamically favourable products of methane oxidation as shown in Figure 2.1. The goal, therefore, is to design a catalyst that facilitates methane oxidation under mild reaction conditions and protects methanol from further oxidation. As will be discussed in section 2.3, this introduces new challenges such as how the catalyst can be activated by an oxidant and how methanol once formed on the the catalyst surface can be liberated.

Conceptually, one may glance at nature and get inspired by the functions in natural enzymes when searching for promising catalytic materials. Methane monooxygenase

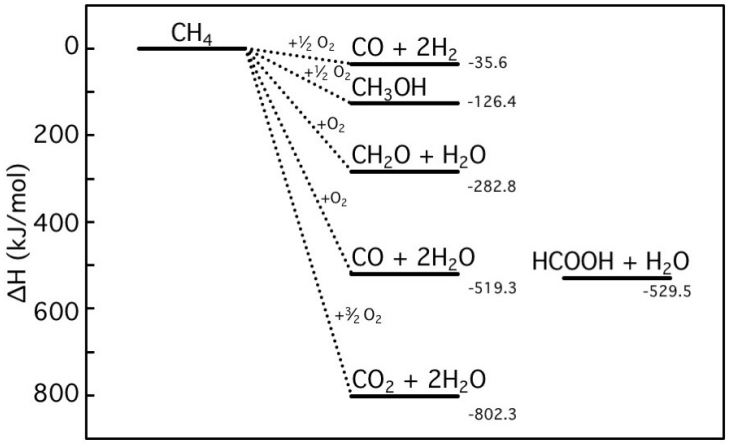

Figure 2.1: Diagram of reaction enthalpies for methane oxidation to various products. All values used in the calculations are standard enthalpy changes of formation of the gas phase compounds.

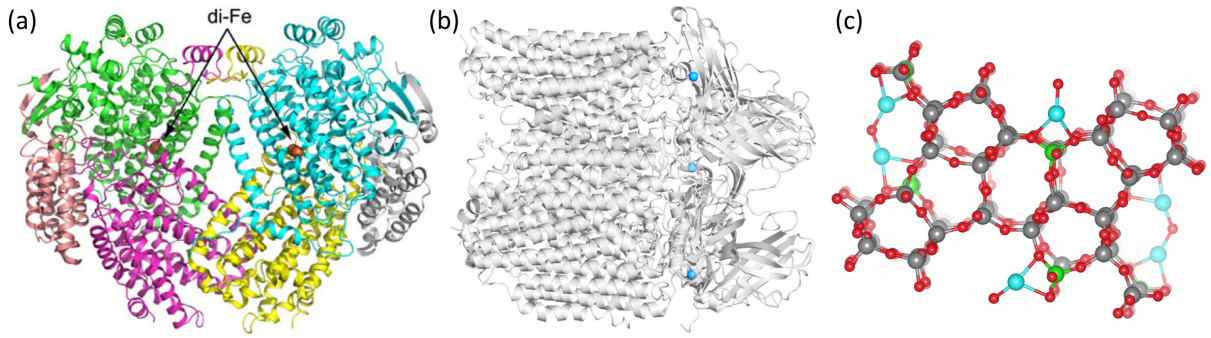

Figure 2.2: Models of structures for catalysing methane to methanol; a comparison between the enzymes and a heterogeneous catalyst. (a) Crystal structure of soluble MMO from Methylococcus capsulatus adapted from reference[14]; the di-iron centres are shown as spheres. (b) Crystal structure of particulate MMO from Methylocystis adapted from Protein Data Bank in Europe[16]; the copper centres are highlighted in blue. (c) Structure model for Cu-ZSM-5; the copper centres are highlighted in blue.

(MMO) is a group of enzymes that can selectively oxidise methane to methanol under ambient conditions. The active site is a di-iron centre in soluble MMO[14] and a copper centre in particulate MMO[15], in both cases with a ligand environment formed by surrounding peptides as shown in Figure 2.2a and b. By designing catalysts hosting active sites that mimic the metal centre and its surrounding structure in MMOs, high selectivity for methanol may be achieved at mild conditions, *i.e.*, at low temperature and ambient pressure. Inspired by the structure of MMOs, researchers have synthesised and tested various metal-exchanged zeolites. An illustration of Cu-ZSM-5 is shown in Figure 2.2c presenting the dicopper active sites surrounded by porous zeolite framework. This type of metal-exchanged zeolites has shown promising selectivity towards methanol. Hitherto, however, they are far from applicable in industrial processes. The challenges regarding metal-exchanged zeolites will be discussed more deeply in Chapter 2.3.

As this thesis mainly focus on experimental studies of copper containing zeolites and zeotypes for methane to methanol, the background and literature review will be focused on related materials and the experimental observations. However, one should bear in mind that the development of heterogeneous catalysts for partial oxidation of methane to methanol cannot be separated from the many theoretical studies. Especially, the identification of active sites is largely dependent on first-principles calculations. These studies, however, are not summarised here. For further interest, I recommend a minireview by Kulkarni *et al.*[17]. Moreover, heterogeneous catalysts are not the only solution to methane conversion to methanol. A number of studies have also found promising results in homogeneous catalysis[18]. Typically, a soluble catalyst is used in a acidic solution for methanol production. The majority of the studies are conducted on noble metal (Pt, Pd, Au, Rh, Os) or Cu, V, Mo based compounds. The progress and limitations, however, in homogeneous catalysts for methane to methanol will not be further discussed in this thesis.

2.1 Heterogeneous catalytic materials

The long-term goal in methane to methanol conversion is to carry out the reaction more efficiently using a heterogeneous catalyst operating under mild conditions. Among the possible catalytic materials, transition metal-exchanged zeolites can already realise this reaction to some extent. They are able to facilitate partial oxidation of methane to methanol under atmospheric pressure and reasonable temperatures. The amount of produced methanol, however, is small and the majority of the studies were not conducted under catalytic (continuous) conditions but instead under quasi-catalytic reaction conditions. This is discussed in Chapter 2.2.1 and 2.2.2.

Besides the transition metal containing zeolites, materials based on molybdenum and vanadium can with even higher methanol yield catalyse methane to methanol but only at elevated temperatures, above 450 °C, and with lower methanol selectivity[18]. As an alternative to conventional heterogeneous catalysts, research on methane to methanol has also been carried out on catalysts based on metal organic frameworks[19], Fe-O embedded graphene[20], nickel-ceria[21] as well as by photocatalytic routes[22–24] and by using dielectric barrier discharge[25–27]. These approaches are beyond the scope of this thesis, which is focused on copper containing zeolites, zeotypes and silica.

2.1.1 Zeolites and zeotypes

Zeolites are microporous materials with a pore size below 2 nm and consist mainly of aluminium, silicon and oxygen. The primary building unit (PBU) for all zeolites is the tetrahedral TO_4 structure where the T-atom, the atom at the centre of the tetrahedral structure, is either Si or Al, as shown in Figure 2.3. The secondary building unit (SBU) is constructed by combining the TO_4 tetrahedrons where the oxygens at the corners of each PBU are shared. By combining different SBUs in various ways, unique zeolite

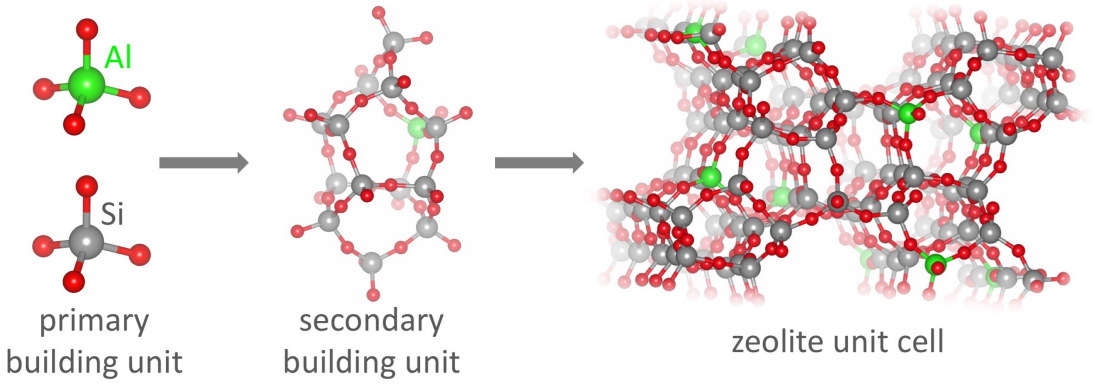

Figure 2.3: From left to right: the T-atoms in its tetrahedral structure forming the primary building unit of zeolite; one type of secondary building unit structures for zeolite; zeolite unit cell (MFI framework structure).

framework structures can be constructed. At present, more than 200 types of framework structures of zeolites have been identified[28], some of which are naturally occurring minerals. Zeolites can accommodate cations (not shown in Figure 2.3) that compensate the negative charge introduced by the aluminium atoms. These cations can be exchanged to desired elements/species with positive charge, which enables steering of the catalytic properties of zeolites. One example is the H^+ containing zeolites that possess Brønsted acidity due to its ability to donate protons. Moreover, each zeolite framework structure is unique, which allows zeolites to favour certain molecular shapes of the reaction products leading to specific selectivity when used as catalysts[29].

Zeotypes are materials with the same framework structures as zeolites but consist of other T-atom combinations than that of the zeolites, *i.e.*, the Si and Al. Besides the large varieties of cation and framework structures, the elements and composition in the zeotype framework can also decide the properties of a zeotype. The high flexibility in adjustable properties has made zeotypes interesting for the purpose of catalysis. One specific zeotype property investigated in this work is the acidity, which can be adjusted by changing the composition of framework T-atoms[30].

2.1.2 Copper-exchanged zeolites/zeotypes and Cu/silica

Since the observation of methanol formation from methane over copper-exchanged zeolites, intensive work has been devoted to, on the one hand, identifying the catalytically active site and, on the other hand, completing the catalytic cycle. Cu-ZSM-5 is the first studied copper containing zeolite for partial oxidation of methane to methanol. With the selectivity as high as 98% towards methanol[31,32], Cu-ZSM-5 starts to attract attention as a promising candidate. Some studies found a correlation between an absorption band at 22 700 cm^{-1} in the ultraviolet-visible (UV-vis) spectral region and the amount of methanol formed during reaction[32,33]. A following study combining Raman spectroscopy, first-principles calculations and normal coordinate analysis calculations identified the origin of the absorption band at 22 700 cm^{-1} as a bent mono-(μ-oxo)dicupric site (illustrated in Figure 2.4a), which therefore has been suggested to be the active site for methane to methanol in Cu-ZSM-5[31]. This suggested active site resembles the oxygen activated di-cupper intermediate in particulate MMO, which is believed to the site for C-H bond activation[34]. A later study showed the quantitative structure-performance relationship between the intensity of the spectroscopic feature at 22 700 cm^{-1} and the methanol production[35]. Guided by the active site assignment, strategies creating higher concentration of the mono-(μ-oxo)dicupric cores, such as controlling the distribution of framework Al[36] or passivating the exchange sites at the external surface of the zeolite grains[37], have been carried out. Though these studies succeeded in controlling the Cu species to some extent, the methanol production is not significantly improved

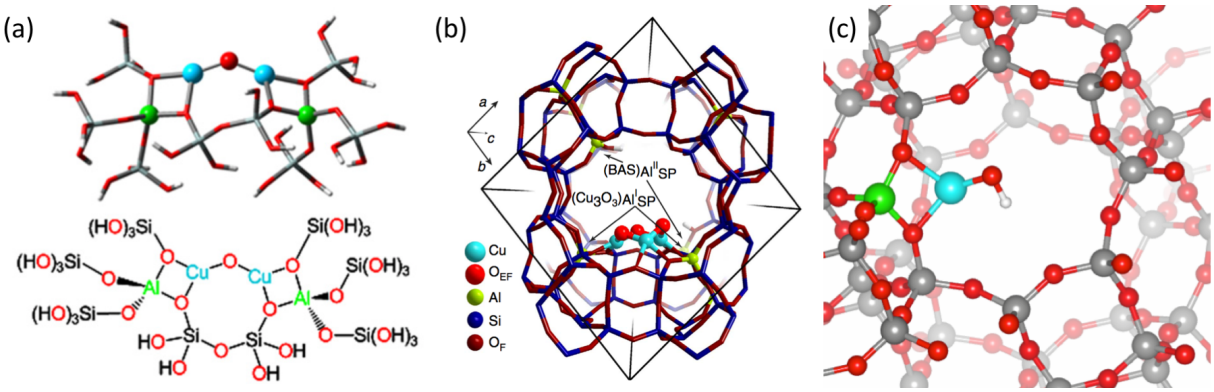

Figure 2.4: Illustration of selected active sites proposed for methane to methanol in Cu-zeolite. (a) Cu dimer in Cu-ZSM-5, adapted from reference[31]. (b) Cu trimer in Cu-MOR, adapted from reference[40]. (c) Cu monomer in Cu-exchanged CHA.

due to the fact that methanol is still produced under stoichiometric reaction conditions. Meanwhile, some researchers are experimenting in completing the catalytic cycle for methane to methanol. An isothermal gas-phase system is found to be feasible for methane to methanol over Cu-ZSM-5[38]. This is later followed by the first realisation of methane to methanol under catalytic conditions, *i.e.*, constant gas composition and temperature[39].

Unlike Cu-ZSM-5, the identification of active site in copper mordenite (MOR) is not as straight forward due to the observation of different spectroscopic changes under similar reaction conditions. One would first anticipate a dicopper site in Cu-MOR similar to the mono-(μ-oxo)dicupric sites identified in Cu-ZSM-5. Such Cu species has been observed experimentally[41–46] and calculated theoretically[42,45] with certain variations according to the reaction conditions. Presented studies have reported different reactivity towards methanol over Cu-MOR depending on the reaction temperature[33] and activation conditions, such as the oxidants used[43] or the presence of water[45]. The results indicate the existence of more than one type of active site. Moreover, a tricopper core (shown in Figure 2.4b) has been proposed and investigated as active sites in Cu-MOR[40,43], while methane to methanol reactivity related to small copper clusters in mordenite was also observed under an isothermal conditions[47]. In contrast to other copper zeolites, Cu-MOR is able to oxidise methane anaerobically by utilising the oxygen in water[48], and an oligometric copper species is proposed to be responsible for methanol production under anaerobic conditions[49]. Possibly, these reports and cases suggest a higher flexibility in catalyst design than first suggested in the early studies on Cu-ZSM-5 catalysts.

Small-pore zeolites and zeotypes have also been tested for partial oxidation of methane to methanol. The Cu-CHA (chabazite) and Cu-SAPO (silico-alumino-phosphate) were the first materials to be reported to exhibit higher production of methanol in com-

parison to Cu-ZSM-5[50]. It was discovered later that zeolites that to a majority consist of 8-membered rings (MRs) while excluding 6, 10 or 12 MRs can host higher concentrations of Cu sites active for methanol formation[51,52]. Both Cu monomers[53] and dimers[51] have been proposed to be active sites for Cu-CHA. Figure 2.4c presents an illustration of a plausible active site, Cu-OH, in chabazite framework. Additionally, Cu-SSZ-13 (CHA) was reported to convert methane to methanol catalytically using N_2O as oxidant[54]. This marks the second material (after Cu-ZSM-5) realising the catalytic cycle of methane to methanol under mild conditions.

Besides the massively studied MFI, MOR and CHA framework structures, the activity towards methanol of many other copper containing zeolite framework structures were studied and compared[52]. Factors such as Si/Al ratio and pore size are found to be important for methanol production. Interestingly, also silica supported copper has been reported to be active for partial oxidation of methane to methanol[55–57]. The effect of reaction conditions and material compositions were investigated thoroughly[55]. Highly dispersed CuO species were identified as the active sites for methanol formation[57]. The observations in these studies suggest that zeolite/zeotype systems are not necessary for supporting copper species active for methane to methanol, as will be shown in this thesis.

2.1.3 Other metal-containing zeolites

Iron zeolite is the earliest model catalyst used for partial oxidation of methane to methanol inspired by MMOs[58,59]. Early studies have explored topics such as modelling of the active sites[60,61], using molecular oxygen for catalyst activation[62] and exploring the mechanisms[63–67]. The active site for methane to methanol was later identified with combined spectroscopic experiments and first-principles calculations as a iron monomer with square planar geometry called α-Fe(II).[68] An α-O site active for methane dissociation can be formed upon activation of such α-Fe(II) with N_2O. At temperatures over 200 °C, methane conversion to methanol can be realised catalytically over Fe-ZSM-5.[64]

Studies on partial oxidation of methane to methanol over Co-ZSM-5 started less than ten years ago and have not drawn much attention since. Mainly molecular oxygen was used as oxidant for methane oxidation. Selectivity towards methanol was reported to be related to larger cobalt oxide domains; while selectivity towards formaldehyde, as the other main product, is associated with cobalt ions at the ion-exchange positions[69,70]. Understanding of topics such as reaction mechanisms[71] and the influence of zeolites pore structures[72] are progressing slowly.

2.2 Operational conditions

2.2.1 Catalytic process

The most common industrial catalytic processes operate under certain catalytic conditions where reactants are fed continuously through the catalyst bed and the temperature profile is steady. For methane to methanol over copper containing zeolites, however, a catalytic cycle has not been realised until recently[39,54]. The comparison of the catalytic cycle and the conventional quasi-catalytic cycle (see Section 2.2.2) is shown in Figure 2.5. Under catalytic reaction conditions, it is possible to study the reaction kinetics including the reaction order of reactants and activation barriers. The methane reaction order over Cu-ZSM-5[39] and Cu-SSZ-13[54] has been calculated to be of around one using experimental data. The dependence on the partial pressure of the oxidants (O_2 or N_2O) is fairly low. The apparent activation energy for methane oxidation ranges from 47 to 149 kJ/mol for Cu-ZSM-5, Cu-MOR[39] and Cu-SSZ-13[54]. The selectivity towards methanol is 71% for Cu-ZSM-5[39] and lower than 40% for Cu-SSZ-13[54].

2.2.2 Quasi-catalytic approach

The usual approach of gas phase partial oxidation of methane to methanol relies on a quasi-catalytic process (shown in Figure 2.5 right panel) consisting of three sequential steps:

Activation Creation of active sites by oxidative treatment of the catalyst at elevated temperature

Reaction Cooling of the catalyst to the reaction temperature with subsequent exposure to methane in the absence of oxidants

Extraction Methanol recovery by feeding water, ethanol or some other solvent, at reaction temperature or lower.

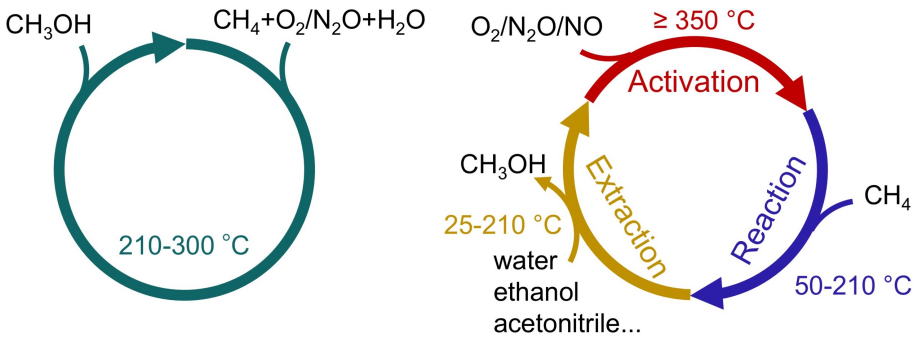

Figure 2.5: The reaction conditions of the complete catalytic cycle (left) and the quasi-catalytic cycle (right).

A selectivity of 98% towards methanol can be reached with this approach.[56] Many studies suggested an increased methanol production when the partial pressure of methane is increased[47,53,73]. Moreover, it is reported that the amount of methanol produced is linear to the activation temperature of the first step for Cu-SSZ-13 and Cu-MOR[52,53].

2.3 Challenges in catalytic conversion

The challenges in partial oxidation of methane to methanol can be summarised in two aspects: obtaining catalytic species active for methane dissociation and controlled oxidation to methanol. Normally, activation of methane is considered difficult due to its strong and localised C-H bond (413 kJ/mol)[74]. For transition metal containing zeolites, however, methane dissociation can be carried out at comparatively low temperatures (typically below 250 °C). In this case, dissociation of oxidants to form active species for methane activation at such low temperature is a critical step. Moreover, the requirement for methane dissociation is rather contradictory to controlled partial oxidation to methanol, as the reaction intermediate can easily undergo further oxidation. While high energy input would not be desirable, the mission lies on finding a suitable catalyst for methane dissociation.

The ion-exchanged zeolite catalysts designed today could resolve both challenges to some extent. These materials, however, have their own limits, which in turn bring other challenges. The approach for gas phase partial oxidation of methane to methanol nowadays mainly relies on the activation-oxidation-extraction sequence, which, strictly speaking, is a stoichiometric reaction rather than a catalytic cycle. Although catalytic production of methanol is possible in some specific cases, the methanol production rate is extremely low (below 55 μmol g^{-1} h^{-1}) and water vapour is still required in the gas feed for methanol extraction.[39,54] Therefore, it is essential to identify and understand these challenges thoroughly for the purpose of designing a realistic catalyst for methane to methanol. For the following discussion, a simplified reaction mechanism for the quasi-catalytic process is shown in Figure 2.6. The widely discussed copper dimer motif is used here for illustration. It should be noted that this reaction mechanism is merely an aid to understand the challenges of partial oxidation of methane to methanol, and it is not a mechanism being calculated theoretically or observed experimentally.

2.3.1 Catalyst activation

In order to obtain and restore the active sites that contain highly active oxygen/hydroxyl groups in functionalised zeolites which could activate the C-H bond in methane, activation of the materials with oxidants (O_2, N_2O or NO) under elevated temperature is often needed. This results in a non-isothermal reaction sequence. It is, however, pos-

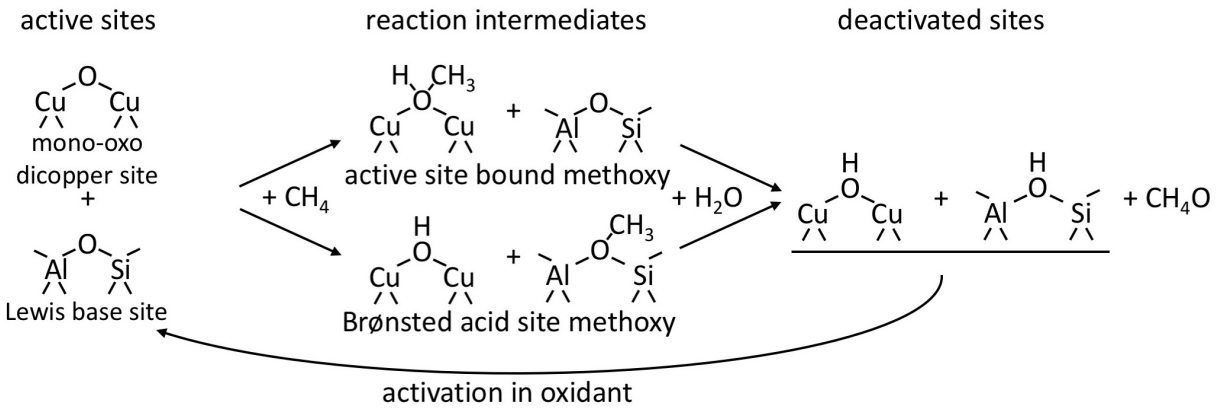

Figure 2.6: A simplified methane to methanol reaction mechanism using the quasi-catalytic approach over a Cu-zeolite. The well studied Cu dimer sites are used here for illustration.

sible to observe low-temperature (150-200 °C) isothermal reaction using a specific oxidant (NO)[38], under elevated methane partial pressure[47] or with compromised reaction rate[39]. Generally, higher activation temperature promotes methanol production.[52,53] The characteristics of the active sites and the changes they may go through during the reaction are yet to be explored.

2.3.2 Active sites for methane dissociation

Once the active sites are formed, the functionalised zeolites are able to convert methane to methoxy stoichiometrically under non-oxidising environment[32,33,35,38,39,75]. The absence of oxidants during the reaction step may be a reason why high methanol selectivity can be achieved. Even though continuous production of methanol is possible in specific cases, the reaction rate is extremely low[39]. Both the concentration of the active sites and the regeneration of them are limiting factors to methanol formation. For Cu-ZSM-5, only approximately 5% of the copper in the material contributes to methanol production[32,33]. Many copper structures have been proposed to be the active sites in various zeolite framework structure. The universal requirements of a site being active for methane to methanol, however, is still unclear. Therefore, it is challenging to design a catalyst with higher concentration of active sites. Meanwhile, the methoxy species formed over the active sites (Figure 2.6 reaction intermediates) terminates its ability to continue to catalyse the dissociation of methane. Therefore, active sites regeneration is closely related to product removal and catalyst activation.

2.3.3 Methanol extraction

After methane dissociation, the formed methoxy species can be adsorbed over the active sites or the Brønsted acid sites (see Figure 2.6 reaction intermediates), the later of which is observed experimentally using IR spectroscopy.[48] It is recognised that such Brønsted

acid sites bonded methoxy is fairly stable.[76,77] To form the final product methanol from methoxy, chemical extraction is necessary. Therefore, addition of proton to the methoxy groups as well as replacement on the methoxy bonded catalytic sites are essential for methanol production. In such case, the stability of the adsorbed methoxy groups becomes a barrier for methanol formation. Consequently covering of active sites with extractant species terminates the reaction, as shown in Figure 2.6, deactivated sites.

2.4 Thesis scope

This thesis presents evaluation of copper zeolites as catalysts for partial oxidation of methane to methanol carried out under quasi-catalytic conditions. Special emphasis is on mechanistic understanding using desorption experiments and first-principles calculations to clarify the interaction of methanol with the catalysts and the need of the extraction step for methanol production over copper zeolites and zeotypes. With this as a base, the last part of the work is focused on tuning the acidity of zeotypes for improved partial oxidation of methane to methanol.

CHAPTER 3
EXPERIMENTAL METHODS

3.1 Sample preparation

3.1.1 Synthesis of zeolite/zeotypes

To synthesise zeolites and zeotypes, several components are needed: a silicon source, other framework element sources (if necessary), a structure directing agent (SDA) and chemicals for pH value adjustment. The detailed synthesis conditions of the boron silicate as well as iron and/or aluminium silicate are described in Paper IV and V, respectively. Five zeolite/zeotype samples were synthesised for this study: a boron silicate with chabazite structure and four silicates (Si, Fe+Si, Al+Si and Fe+Al+Si) with MFI structure. For the boron silicate sample, an SDA solution was prepared and adjusted to basic condition. The boron and silicon sources were then added with 15 minutes gap between each addition. The structure of the boron silicate is shown in Figure 3.1a. For the Fe and/or Al silicate, solutions of silicon source and certain metal source(s) were prepared separately and then mixed together after certain time according to the zeotype being synthesised. For the iron containing samples, an acidic environment is necessary to avoid metal hydroxide precipitation. The SDA was then added and the gel was adjusted to basic condition for crystallisation. Generous amount of time was given for stirring at each step. The gels for all five samples were then kept in autoclaves at constant temperature for certain days. The resulted products were finally washed and dried.

3.1.2 Functionalisation of zeolites, zeotype and silica

Two preparation methods, *i.e.*, incipient wetness impregnation and aqueous ion-exchange, have been employed in order to obtain powder samples containing metal nanoparticles

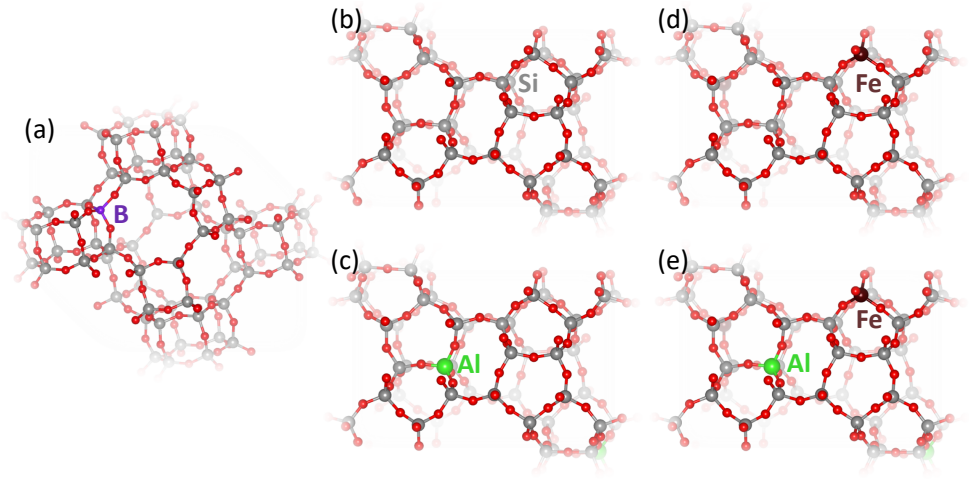

Figure 3.1: Structures of the five zeotype/zeolite samples synthesised in this work. (a) boron silicate with CHA structure, (b) silicate with MFI structure, (c) aluminium silicate with MFI structure, (d) iron silicate with MFI structure, (e) iron aluminium silicate with MFI structure.

and isolated metal species, respectively. The powder samples are wash-coated onto monolith substrates and used for flow reactor studies as described in Chapter 3.2.

Incipient wetness impregnation

For incipient wetness impregnation, a dry powder (often the support material) is mixed with a solution containing the precursor of the active phase. The solution is added drop-wise. The volume of the solution needs to be equivalent to the pore volume of the powder to be mixed with, in order to achieve a homogeneous impregnation of the support and thus even distribution and dispersion of the active phase. Finally, the powder is freeze-dried and calcined. A desired metal loading can be managed using this method. The resulting impregnated and calcined sample often contains metal nanoparticles. The silica supported copper sample discussed in this work was prepared using incipient wetness impregnation. Details of the metal loading and calcination conditions are described in paper I.

Aqueous ion-exchange

For introducing copper to the zeolite as charge-compensating cations, aqueous ion-exchange (AIE) is often used. The parent zeolite is mixed with an aqueous copper salt solution and stirred for certain time to facilitate ion-exchange. The ion-exchange can be prepared at elevated temperature. The pH value of the solution is often kept at certain value to avoid damage on the structure of the support material and precipitation of copper species. Finally, the liquid is filtered, washed and dried. If preparation conditions such as ion-exchange time and temperature are adjusted suitably, it is possible to achieve a powder sample with well dispersed metal ions. All copper zeolite and zeotype samples were prepared using AIE as described in paper I-IV.

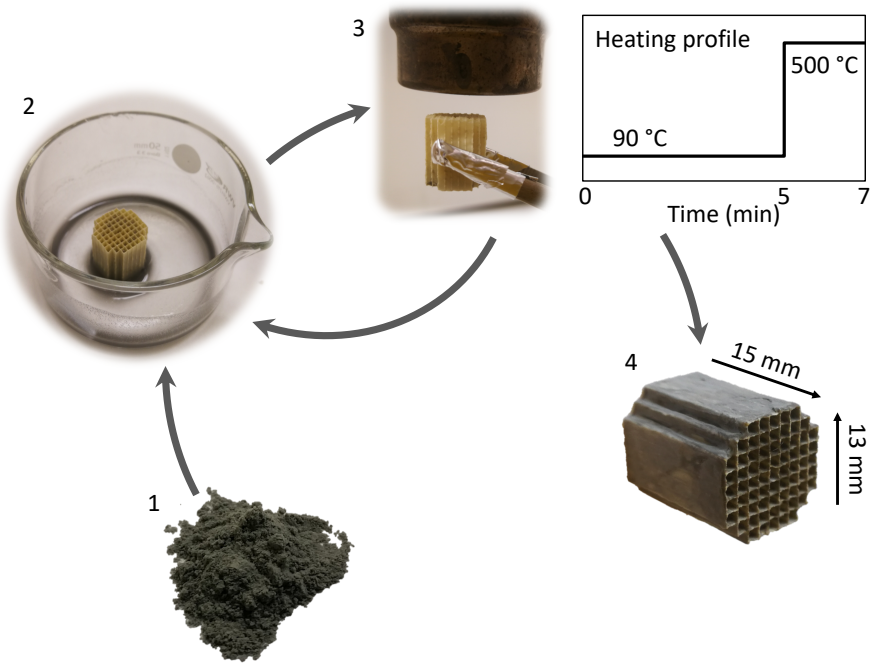

Figure 3.2: An example of a wash-coating procedure. The powder sample (1) is made into a slurry where a monolith substrate is dipped in (2). The monolith is then calcined with certain heating profile (3). Step 2 and 3 are repeated until the wash-coat reaches 0.2 g. The resulting wash-coated monolith sample (4) is eventually calcined in oven.

3.1.3 Monolith coating

For flow reactor studies, the powder samples are often wash-coated on a monolith substrate following the procedure shown in Figure 3.2. During this process, a cordinite monolith with certain dimensions (Corning, 400 cpsi, L=15 mm, Ø=13 mm) is dipped in a slurry containing the powder sample, a binder (Sasol, Disperal P2) and Milli-Q water. The monolith is then dried with a heating gun in air at 90 °C for 5 min followed by quick calcination in air at 500 °C for 2 min. The calcined monolith substrates are coated with thin layers of the wash-coat until the added solid material on each substrate reached 0.2 g. The monolith samples are finally calcined in air at 600 °C for 3 h.

3.2 Chemical flow reactor measurements

A chemical flow reactor system compatible for monolith samples was used both for evaluating catalytic activity/selectivity of the copper based materials and for speciation of the gas phase composition during temperature programmed desorption (see Section 3.2.2). The sample environment of the flow reactor is illustrated in Figure 3.3. It consists of a horizontally mounted fused quartz tube surrounded by a heating coil for resistive heating, which is wrapped in quartz wool for insulation. The monolith sample is positioned close to the gas outlet between two uncoated monolith substrates that low-

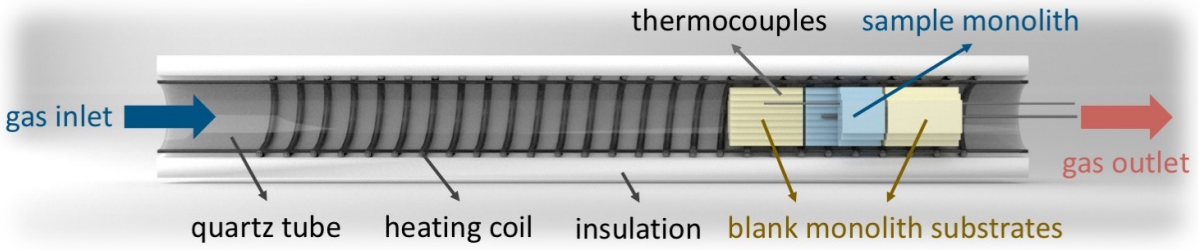

Figure 3.3: Illustration of a flow reactor. The gas mixture from mass flow controllers (not shown) flows in a horizontally mounted quartz tube (covered with heating coil and insulation) to the sample monolith, and eventually flows out from the quartz tube for composition analysis. The sample monolith is positioned close to the outlet end in between of two blank monolith substrates for reducing temperature and concentration gradients. The reactor temperature is controlled and monitored by a thermocouple in one channel of the front blank monolith substrate. The catalyst temperature is measured by another thermocouple in the middle of the sample monolith.

ers radiation heat losses and create a more isothermal sample. The temperatures of the inlet gas and catalyst sample is measured by thermocouples (type k) positioned inside the upstream uncoated monolith substrate and inside the sample monolith, respectively.

The gas feed is composed by a gas mixing system that consists of several mass flow controllers (Bronkhorst Hi-tech) for gases (O_2, N_2O, NO, CH_4 and Ar as carrier) and a controlled evaporator mixer (Bronkhorst Hi-tech) and a controlled evaporator mixer device (Bronkhorst Hi-tech) for injection of liquids (CH_3OH). Also, a separate water generator that produces ultra-pure water vapour from catalytic reaction between H_2 and O_2 was connected to the gas feed[78]. This is a convenient approach to supply water while minimising the risks of contamination (*e.g.*, by ions) when using water from a water reservoir during product extraction. The gas mixing system and reactor heating are controlled and monitored by use of an in-house coded Labview (National Instruments) control program. The gas phase species from the gas outlet are analysed by a Fourier-transform infrared (FTIR) spectrometer operating in transmission mode (MKS Instruments, MultiGas 2030). The basic theory of FTIR is explained in Section 3.4.1. The use of monolith samples in the flow reactor ensures low pressure drop and compatibility with high gas flow rate, which is needed for the downstream FTIR analysis.

3.2.1 Activity-selectivity test

The activity test for methane to methanol is carried out in the flow reactor through the activation-reaction-extraction sequential approach shown in Figure 3.4. The samples are activated at 550 °C with oxidants (20% O_2, 300 ppm N_2O or 0.1% NO) for one hour before oxidation of 2% CH_4 at 150 °C. The products are then extracted with water vapour at 150 °C. The flow is kept at 750 ml/min during the activation and reaction steps, and at 300 ml/min during the extraction step. The lower flow rate for

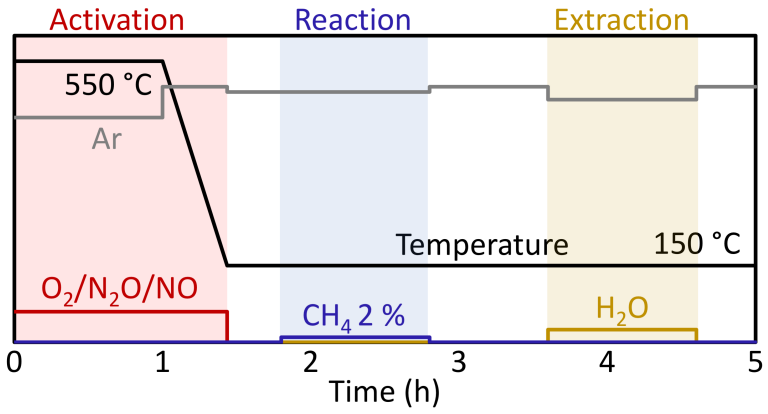

Figure 3.4: The quasi-catalytic reaction conditions for partial oxidation of methane to methanol in a chemical flow reactor system. Activation: at 550 °C for 1 h and subsequently cooling to 150 °C in oxidants. Reaction: methane reaction for 1 h at 150 °C. Extraction: water extraction for 1 h at 150 °C.

the extraction step as well as the quasi-catalytic approach was employed on the purpose of increasing the methanol concentration for FTIR detection, as the extremely low methanol production for this reaction reaches the lower edge of the instrument detection limitation. Methane concentration from early studies (1-10% CH_4)[31,33,38,79] was taken into consideration for the choice of the reaction step condition in this study.

3.2.2 Temperature-programmed desorption

Though there are reported examples of catalytic methane to methanol with compromised methanol production[75] or selectivity[54], the majority of the study of methane to methanol focus on the quasi-catalytic process due to the higher methanol production and selectivity. It is extremely difficult to study the reaction kinetics under such a reaction sequence. Furthermore, extraction of methanol remains a "black box" and may be a key to avoid the activation-oxidation-extraction sequence. Therefore, in this study the interaction between methanol and Cu-ZSM-5 was explored using methanol temperature-programmed desorption (TPD). The flow reactor system is used to probe desorbed gas phase species during the desorption phase of the TPD experiment.

TPD can be used to gain information about certain interactions between the adsorbate(s) and the surface including the surface sites. The principle result of a TPD measurement is illustrated in Figure 3.5. Before the TPD experiment, the surface of the sample is annealed and/or prepared by oxidative/reductive treatment (Figure 3.5a) followed by adsorption of the actual probe molecule(s) at low temperature (Figure 3.5b). The sample is flushed by inert gas for desorption of weakly bound probe molecules and then a linear heating rate is applied to desorb the chemisorbed probe molecules into the gas phase, which is analysed by suitable analysers such as FTIR or mass spectrometer. An example of a TPD profile is shown in Figure 3.5c. This specific example

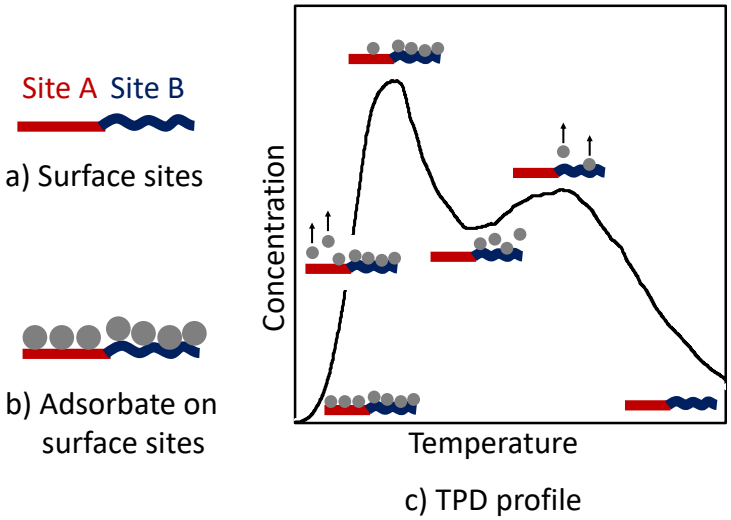

Figure 3.5: Schematic sketch of TPD: a) a simplified clean surface with two types of adsorption sites A and B; b) surface covered with absorbate after adsorption; c) TPD profile with illustration of desorption of the adsorbate from the surface.

illustrates the TPD profile of a simplified surface with two types of adsorption sites, weak adsorption on site A and strong adsorption on site B. With increasing temperature, the adsorbate weakly bound to site A starts to desorb followed by desorption of the adsorbate more strongly bound to site B at higher temperatures. Two peaks are therefore formed in the TPD profile, which relate to these two sites. Generally, different peak desorption temperatures indicate different types of adsorption sites, while the area under the peak is proportional to the number of adsorption sites. TPD analysis thus gives information about the type and number of adsorption sites. Moreover, the kinetic order and desorption energy can be extracted from the TPD profiles. Through shape analysis of the asymmetry of a single component TPD profile and parameter fitting, information about the desorption order can be achieved[80]. The desorption energy can be obtained by methods such as complete analysis[81], leading edge analysis[82], Redhead analysis[83] and by varying the heating rate[84]. In general, methods in which the desorption energy and the frequency factor (*i.e.*, pre-exponential factor) are assumed to be independent of the coverage, such as in the Redhead analysis, tend to introduce errors in the estimated desorption energy whereas methods that consider coverage dependent parameters result in more accurate values. The complete method is an example of the latter, however, it requires considerably larger efforts for the analysis. For a broader overview and comparison of thermal desorption analysis methods see *e.g.* the work by de Jong and Niemantsverdriet[80].

For the methanol-TPD in the flow reactor, the samples are pretreated in O_2 at 550 °C for 1 h before methanol adsorption at 80 °C until saturation. The desorbed gas phase species were then recorded using FTIR spectrometry during a heating ramp of 5 °C/min.

3.3 *Ex situ* catalyst characterisation

3.3.1 Powder X-ray diffraction

Powder X-ray diffraction (XRD) is commonly used to determine the crystal structure(s) and mean particle size of a material. In this technique, X-ray radiation incident on the spinning sample surface from a range of angles. Reflection of the elastically scattered X-rays are then detected by a rotating detector positioned on the other side of the sample. Reflection occurs only when the scattered X-rays interfere constructively, which is described by the Bragg's Law[85]: $n\ \lambda = 2\ d\ \sin\theta$, where n is any integer, λ is the wavelength of the incident X-rays (nm), d is the spacing between the crystal planes (nm), and θ is the angle between the incident X-rays and the crystal planes ($^\circ$).

In powder samples, different crystal planes are randomly oriented. By scanning a range of incident angles, reflection occurs from planes that are oriented at the correct angle and fulfill the Bragg's Law. From the powder diffraction patterns obtained, the d spacing of each reflection can be calculated. Furthermore, an estimation of the crystal size can be obtained using the Scherrer equation[86].

In this work, XRD is used for confirming the crystal structure of the synthesised boron silicate, the iron and/or aluminium silicate, the copper zeolite and zeotype samples after AIE, as well as determine the crystal structure and mean particle size of the copper particles in the Cu/SiO_2 sample.

3.3.2 Nitrogen physisorption

Nitrogen physisorption is often used for determining the (total) surface area and pore volume of porous materials. The measurement is performed at constant temperature where the volume of nitrogen adsorbed or desorbed is measured at a range of pressures to form adsorption and desorption isotherms. The Brunauer–Emmett–Teller (BET) theory[87] is commonly used for analysing specific surface area. The theory is based on the assumption that a monolayer of the adsorbate is formed on the measured material (adsorbent), followed by the successive layers adsorbed with the adsorption energy equals to the energy of liquefaction. It has to be noted that BET analysis is not strictly applicable for microporous materials, such as zeolites, where a pore filling process accompanies monolayer formation at low pressure, which violates the monolayer formation assumption. The values of BET surface area, however, can still be used for empirical comparisons for the same type of microporous material. In this study, N_2 sorption is used to determine the BET surface area and micropore volume as well as to evaluate the zeolite and zeotype pore structures.

3.3.3 X-ray absorption spectroscopy

X-ray absorption spectroscopy (XAS) is a widely used technique for determining the oxidation state and local structure of selected elements in a material. Thanks to its unique sensitivity of local structure and rather straightforward requirement on sample environment, it has been well established as an *in situ/operando* characterisation method for studying catalysts under realistic reaction conditions. In this work, however, it is used as an *ex situ* characterisation method. XAS measurements are performed at a synchrotron radiation sources as to utilise the intense and tunable X-rays. Figure 3.6a shows one common XAS setup, where the incident X-ray on the sample are scanned through a certain range of monochromatic photon energies. When the incident photon energy is higher than the binding energy of a core electron, the photon is annihilated, transmitting its energy to a core electron creating a photoelectron and a core hole. The core hole is then filled by an electron from a higher energy state releasing fluorescence X-rays. The energy dependent absorption coefficient ($\mu(E)$) is proportional to the measured X-ray intensity, i.e., $\mu(E) \propto \ln {}^{I_0}/_{I_1}$ and $\mu(E) \propto {}^{I_f}/_{I_0}$ for transmission and fluorescence measurements, respectively. Here, I_0 is the incident light intensity I_1 the light intensity after

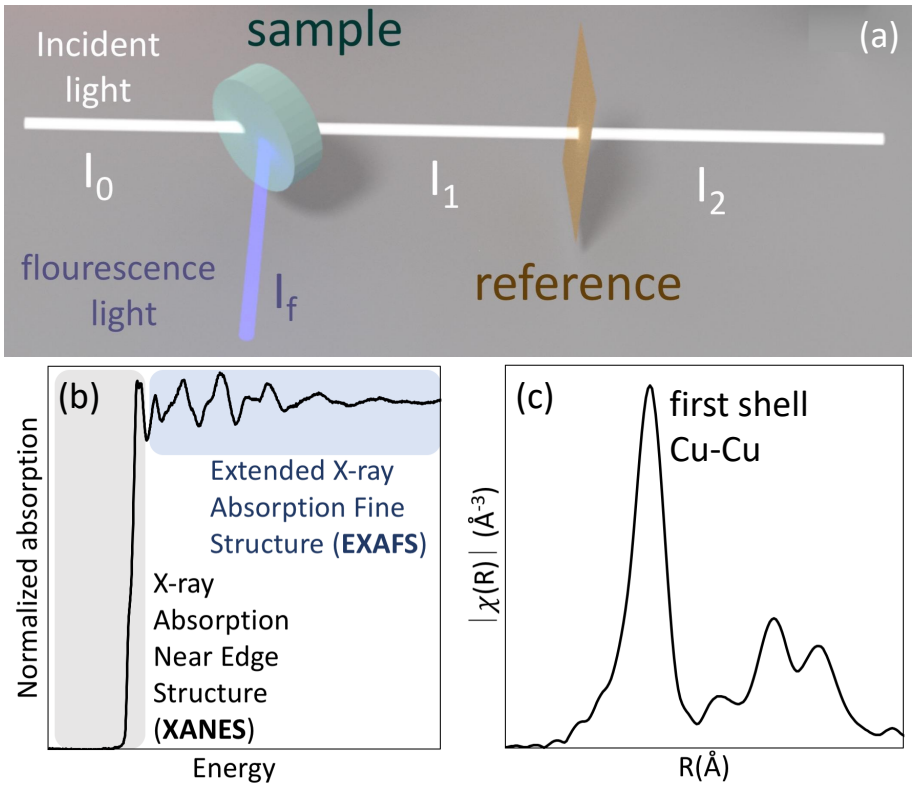

Figure 3.6: (a) Illustration of an XAS setup. The incident beam (light intensity I_0) passes through the sample and subsequently the reference. The light intensity is denoted as I_1 and I_2 after the sample and the reference, respectively. The sample emits fluorescence light with the light intensity denoted as I_f. (b) Normalised X-ray absorption spectrum of Cu foil.(c) Fourier transform EXAFS spectrum from Cu foil.

the sample and I_f the intensity of the fluorescent light.

X-ray absorption spectra are measured around an absorption edge at which core electrons are excited from their bound states to the continuum, resulting in a sharp increase in absorption as shown in Figure 3.6b. The region close to the absorption edge is called the X-ray absorption near edge structure (XANES) region, where the spectrum shape reflects the excitation of core electrons to the final states. In certain XANES spectra, the absorption edge appears to be a sharp intensive peak referred as "white line"[1]. Typically, XANES spectra are analysed by comparing the measured spectrum with spectra of known structures, as so called "fingerprinting". The X-ray absorption spectrum region that is higher in energy than the absorption edge is called the extended X-ray absorption fine structure (EXAFS) region, where the spectrum shape reflects the surrounding structure of the absorbing atoms. Using suitable data processing, the EXAFS is used for obtaining information of different coordination shells. As shown in Figure 3.6c, the peaks of the Fourier-transform of the EXAFS spectrum correspond to the different coordination shells in the Cu face centred cubic crystal structure.

In this work, XAS is used as an *ex situ* characterisation technique for obtaining the coordination chemistry of the copper species in the as-prepared Cu-ZSM-5 and Cu-SSZ-13 samples.

3.3.4 Micro-calorimeter

In catalysis, calorimeter is often used to measure heat changes of a catalyst during adsorption of molecules or a chemical reaction. The micro-calorimeter set-up used in this study is designed to measure heat changes of a powder sample in gas flow and under precise temperature control. To realise heat measurements under such conditions, a differential scanning calorimeter (DSC) equipped with a gas mixing system (consisting of several mass flow controllers) and a mass spectrometer is employed. Two quartz tubes with sintered quartz beds in the middle of the tubes are placed in the DSC, one containing the powder sample to be measured, the other left empty as the reference. The heat flow of the sample is measured by comparing the heat supply of the reference tube and the sample tube under the same temperature.

In this work, micro-calorimeter is used to measure the average heat of ammonia adsorption over zeolites and zeotypes. The detailed procedure is described in Paper IV.

[1] X-ray absorption spectra were recorded on films in the past. The complete absorption of the incident X-ray with certain wavelength during an intense transition leaves a white vertical strip on the negative. Such white strip is called "white line".

3.4 *In situ* catalyst characterisation

3.4.1 Diffuse reflectance infrared Fourier-transform spectroscopy

FTIR spectroscopy is commonly used for identifying functional groups or surface species. This technique is based on the interaction between molecules and infrared (IR) radiation. Transition between vibrational levels of certain chemical bonds may occur upon absorption of IR photons with equivalent energy which can be represented by IR frequency or wavenumber. The transition energy of the vibrational levels depends on the mass of the atoms at each end of the chemical bond as well as the bond strength which can be affected by a range of factors, such as adjacent bonds or structures, adsorption sites or modes, and temperature. This means that the IR absorption frequency is unique for the chemical bonds or functional groups and is sensitive to changes around them. Therefore, IR spectroscopy provides the possibility of identifying different compounds simultaneously as well as observing changes of the targeted species. Figure 3.7 gives an example of a typical IR spectrum discussed in this thesis, where a compound (methanol in this specific case) is adsorbed on a solid material (copper zeolite). According to the bond strength and the atomic weight of the atoms involved, the approximate resonance frequencies (wavenumbers) are predictable. These predicted regions are marked in coloured boxes in Figure 3.7. Moreover, as the absorption wavenumber is sensitive to the adjacent environment of the chemical group/species under investigation, it is possible to obtain information of the sites where the chemical group/species is adsorbed on, as shown in the chemical structures in Figure 3.7.

An FTIR operating in diffuse reflectance mode (diffuse reflectance infrared Fourier-

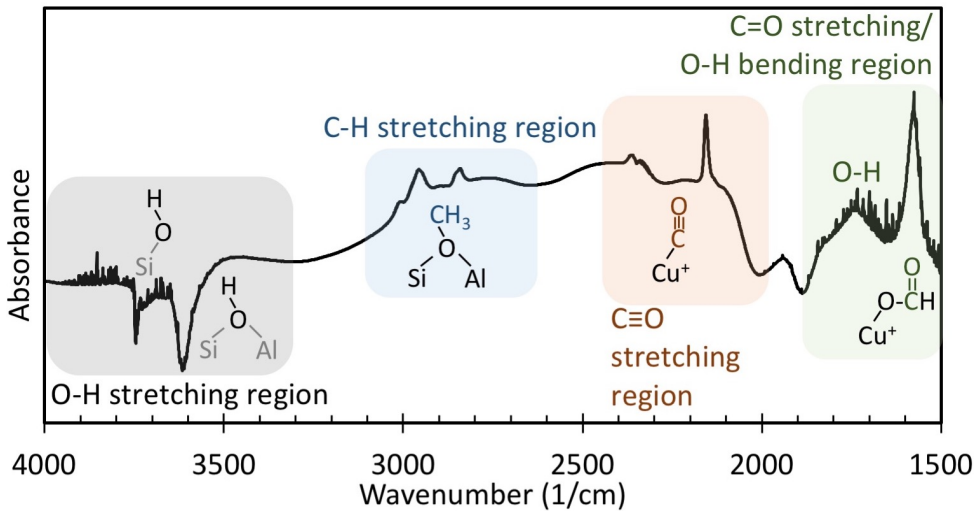

Figure 3.7: Example of an IR spectrum. The spectrum was taken on a copper zeolite sample with methanol adsorbed on the surface. The spectrum is marked with different vibration regions and examples of the corresponding vibrations are given in structure with the related chemical groups marked in colour.

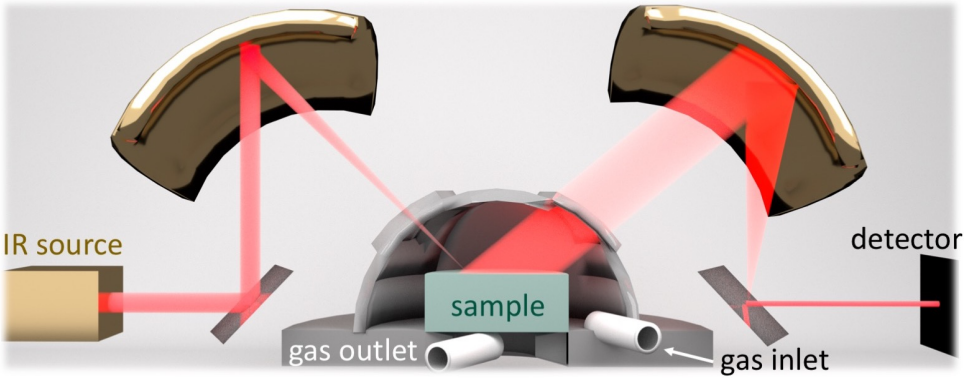

Figure 3.8: Illustration of a DRIFTS setup. The incident beam produced from the IR source is directed to the sample cell. The diffuse reflection of the beam from the sample is then collected and sent to the detector. The sample cell is designed for gas flow and heating.

transform spectroscopy, DRIFTS) is commonly used in catalysis as an *in situ/operando* technique for mechanism study. A simplified illustration of the DRIFTS set-up with emphasis on the sample cell is shown in Figure 3.8. In DRIFTS, a broadband light beam goes through a Michelson interferometer (not shown in Figure 3.8), and is thereafter directed onto the powder sample. The light interacts with the sample and diffuse reflection is generated by the sample's rough surface. The reflected light is collected by optics and directed to the detector. The raw data containing light intensity is eventually collected and Fourier-transformed to a desired spectrum. The *in situ* DRIFTS cell (Praying Mantis ™ High Temperature Reaction Chamber, Harrick Scientific Products Inc.) used in this study is designed for experiments with sample heating and gas flow.

In this work, DRIFTS is used for surface species identification during methane oxidation, methanol-TPD and NH_3/NO adsorption experiments. For the methane oxidation measurements, IR spectra were taken during the reaction and extraction steps of the quasi-catalytic cycles, see Papper I and IV. For the methanol-TPD experiments, the pre-oxidised samples were exposed to methanol at 30 °C followed by step-wise methanol desorption and IR measurements at certain temperatures as described in Paper III. For the evaluation of the acidity of the zeotypes in Paper V, IR measurements were carried out after calcination of the NH_4-zeotypes and NH_3/NO adsorption on the H-zeotypes.

CHAPTER 4

RESULTS AND DISCUSSION

4.1 Methanol formation over Cu-zeolites and Cu/SiO_2

Activity tests in flow reactor of materials containing different Cu species, *i.e.* isolated Cu ions/clusters and Cu nanoparticles, were carried out aiming at comparing the difference in methanol production over these Cu species. To achieve isolated Cu ions/clusters and Cu nanoparticles, zeolites (ZSM-5 and SSZ-13) were ion-exchanged with Cu ions and silica was impregnated with aqueous Cu ion solution. The Cu species in the Cu-ZSM-5, Cu-SSZ-13 and Cu/SiO_2 samples are identified using XRD and XAS, as shown in Figure 4.1a and b. The methanol produced during the extraction step of the quasi-catalytic process over all three samples is presented in Figure 4.1c. The surface species present in the reaction and extraction steps are investigated using DRIFTS and the results are shown in Figure 4.2.

Figure 4.1a shows the XRD patterns of the Cu-ZSM-5, Cu-SSZ-13 and Cu/SiO_2 sample. Characteristic reflections of crystalline CuO, denoted with asterisks, are present in the XRD pattern of the Cu/SiO_2 sample, indicating the existence of CuO particles in the Cu/SiO_2 sample. The XRD patterns of the Cu-SSZ-13 and Cu-ZSM-5 samples, however, exhibit the characteristic peaks of the MFI and CHA crystal structure respectively[28]. No reflections of crystalline CuO species are visible in these patterns suggesting that the Cu species in the Cu-SSZ-13 and Cu-ZSM-5 samples are smaller than 3 nm. The XANES spectra for the Cu-SSZ-13 and Cu-ZSM-5 samples shown in Figure 4.1b overlap with each other. Both spectra present a sharp absorption at about 8995-8998 eV, which is due to the 1s to 4p electronic transition of Cu(II) species[88]. No obvious pre-edge peak for Cu(I) (well defined peak at 8982-8984 eV[88,89]) can be observed, indicating that the oxidation state of the Cu species is dominantly Cu(II) in both samples. The featureless pre-edge, however, eliminates the existence of CuO like structures (weak absorption at

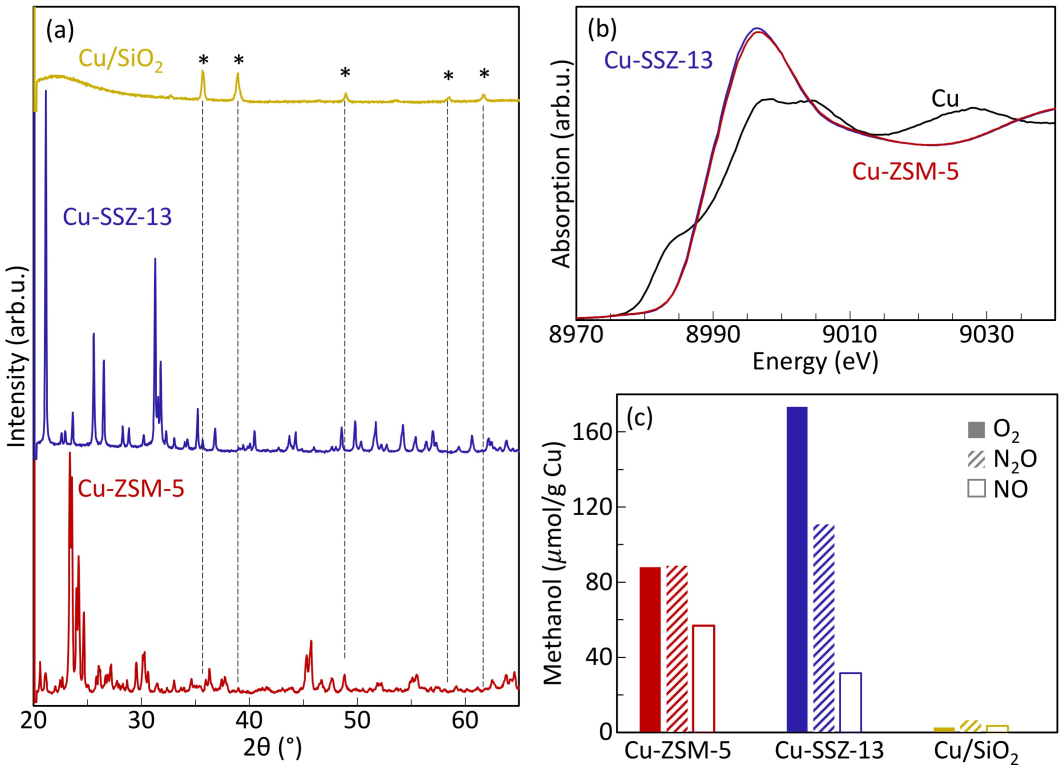

Figure 4.1: (a) XRD patterns for the Cu/SiO_2, Cu-SSZ-13 and Cu-ZSM-5 samples and the parent H-ZSM-5; the characteristic reflections of the CuO crystalline structure are denoted with asterisks. (b) XANES spectra of the Cu-SSZ-13 and Cu-ZSM-5 samples; spectrum of Cu foil is included as reference. (c) Methanol production over Cu-ZSM-5, Cu-SSZ-13, Cu/SiO_2 and H-ZSM-5 using O_2, N_2O or NO as oxidants.

about 8976-8979 eV and shoulder at about 8985-8988 eV[89]), indicating that the Cu-SSZ-13 and the Cu-ZSM-5 samples do not contain detectable amounts of large CuO domains. The XAS results agree with the results from the XRD analysis for the Cu-SSZ-13 and Cu-ZSM-5 sample, suggesting that isolated Cu ions/clusters are the dominant Cu species in both samples.

Activity test for methane to methanol was carried out in the chemical flow reactor system through the quasi-catalytic approach described in Chapter 3.2. Methanol as the main product, is present in Figure 4.1c, where the methanol production is acquired by applying peak area integration to the original methanol FTIR signal during water extraction, followed by subtraction of the amount of methanol produced over the H-ZSM-5 sample with corresponding oxidants. Materials containing different Cu species, *i.e.* Cu ions/clusters or CuO particles, have been tested for methane to methanol with various oxidants. All samples show low amounts of methanol production during water extraction. The methanol production over the Cu-ZSM-5 and Cu-SSZ-13 samples, however, is clearly higher than that over the Cu/SiO_2 sample. The Cu-ZSM-5 and Cu-SSZ-13 samples consist mainly of isolated Cu ions/clusters, ZSM-5 framework sites as well as zeolitic defects, while the Cu/SiO_2 sample dominantly con-

tains Cu nanoparticle site and silica sites. Therefore, the higher methanol production from the Cu-ZSM-5 and Cu-SSZ-13 samples compared with the Cu/SiO_2 sample can be attributed to the isolated Cu ions/clusters, which is in consistency with previous studies[31,33,90–94]. Moreover, the small amount of methanol formed over the Cu/SiO_2 sample regardless of oxidant is an interesting observation. A couple of recent studies also reported activity for methane to methanol of the Cu/SiO_2 system[55,56]. It is speculated that the Cu/SiO_2 sample is not free from isolated Cu ions/clusters which contribute to its activity towards methanol. This is encouraging as the support material for Cu species active for methane to methanol may be much more flexible than it has been recognised before. It should be mentioned that due to the low methanol concentrations, one should be careful with quantitative analysis and instead interpret the experimental activity results in a qualitative manner. It is worth noticing that the amount of methanol produced over the Cu-ZSM-5 sample is similar regardless of the oxidant used during the activation step, while the use of different oxidants results in a considerable difference in methanol formation over the Cu-SSZ-13 sample. For Cu-ZSM-5, the methane to methanol reaction has been correlated (only) with the mono(μ-oxo)dicupric site as characterised by the absorption band at 22 700 cm^{-1} in UV-vis spectrum, while multiple absorption features in the UV-vis[54,95] and Raman[51,53] spectra have been reported for O_2/N_2O activated Cu-SSZ-13, which is indicative of the presence of various Cu species active for methane to methanol. Moreover, the observed UV-vis bands after O_2 and N_2O activation[54] differ, suggesting that each oxidant activates distinct Cu species. This may be the reason for the different amounts of formed methanol observed here when using O_2 or N_2O.

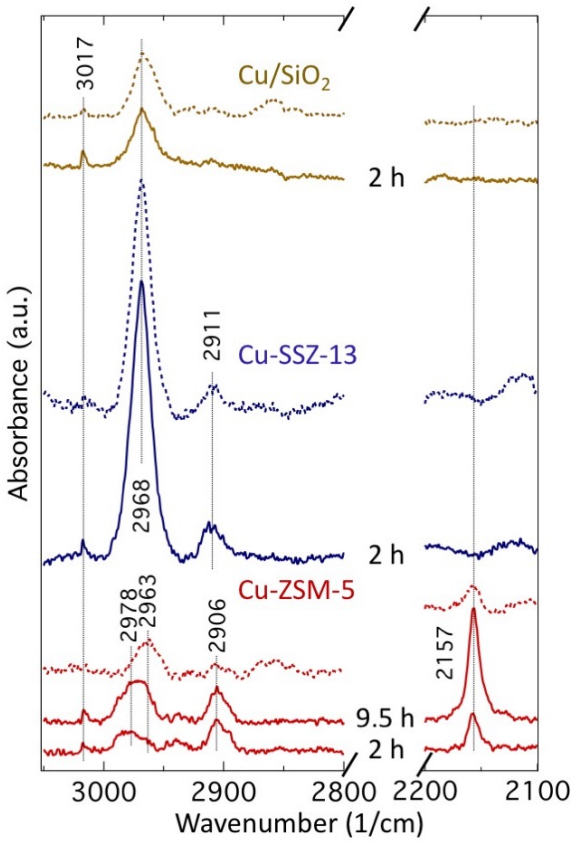

Figure 4.2: IR spectra of pre-oxidised Cu-ZSM-5, Cu-SSZ-13 and Cu/SiO_2 exposed to 2% methane (solid lines) and after water extraction for 10 min (dotted lines) at 250 °C. The activation step was carried out in 500 ppm N_2O for 1 h. All spectra were recorded in Ar.

To further understand the difference in methanol production over the Cu-ZSM-5, Cu-SSZ-13 and Cu/SiO_2 samples, IR measurements were conducted to obtain information of the surface species involved during the reaction and extraction step of the reaction, as shown in Figure 4.2 solid and dotted lines, respectively. For the Cu/SiO_2

sample, under 2 h CH_4 exposure, methane adsorbs dissociatively forming the absorption band at 2968 cm^{-1} [96–99]. For the Cu-ZSM-5 and Cu-SSZ-13 samples, C-H stretching vibrations of the methoxy species contribute to the absorption bands at 2930-3000 cm^{-1},[65,71,76,100] suggesting conversion of methane to methoxy on these two samples after 2 hours exposure to methane. Moreover, CO formation (2157 cm^{-1}) [101] is observed on the Cu sites in the Cu-ZSM-5 sample, indicating that the Cu species in this sample can over-oxidise methane to unwanted species. After water extraction (the dashed lines), all absorption bands decrease in intensity for the Cu-ZSM-5 and Cu-SSZ-13 samples, while no obvious change can be observed in the spectrum of the Cu/SiO_2 sample. It is anticipated that the methoxy species formed on the Cu-ZSM-5 and Cu-SSZ-13 samples react with water and produce methanol, which correlates with the higher amount of methanol detected for the Cu-ZSM-5 and Cu-SSZ-13 samples compared to the Cu/SiO_2 sample in the flow reactor study.

4.2 Methanol desorption from Cu-zeolites

Methane to methanol over heterogeneous catalysts faces many challenges with one in particular: methanol desorption. For a thorough solution to the activation-oxidation-extraction approach, it is necessary to obtain deeper understanding of the extraction step which is crucial for methanol production. By fully understanding it, one could answer question such as weather methanol is formed during methane oxidation and why extraction is needed for methanol formation. Therefore, in this work the interaction between Cu containing materials and methanol was explored using methanol-TPD.

TPD profiles

Methanol and DME are the main species that desorb during methanol-TPD at lower temperatures (below 300 °C). The methanol and DME desorption profiles of the the Cu-ZSM-5, Cu-SSZ-13, Cu/SiO_2, H-ZSM-5, H-SSZ-13 and SiO_2 samples are presented in Figure 4.3.

The desorption profiles of methanol for the Cu-ZSM-5 and Cu-SSZ-13 samples (Figure 4.3 left panel) exhibit desorption peaks with higher intensity and broader width at higher temperatures compared with those for the H-ZSM-5 and H-SSZ-13 samples. The higher intensity of the methanol desorption peaks for the Cu-zeolite samples compared with their parent zeolite samples suggests that the Cu species in ZSM-5 and SSZ-13 are responsible for the additional methanol adsorption, while the methanol desorption at higher temperature for the Cu-zeolite samples indicates that some of the Cu species in ZSM-5 and SSZ-13 interact more strongly with methanol compared to the other sites, *e.g.* Brønsted acid sites and silanol groups, in the zeolite samples. The desorption

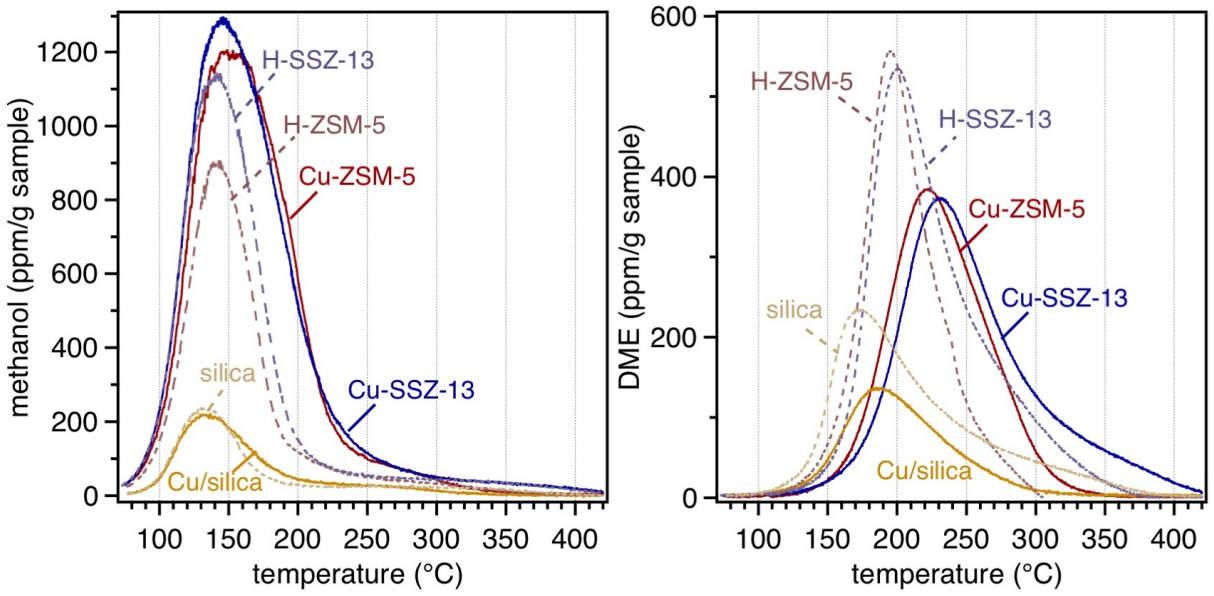

Figure 4.3: Desorbed gas phase species during methanol-TPD from the Cu-ZSM-5 (red solid line), Cu-SSZ-13 (blue solid line), Cu/SiO_2 (yellow solid line), H-ZSM-5 (red dashed line), H-SSZ-13 (blue dashed line) and SiO_2 (yellow dashed line) samples. Left panel: methanol; right panel: DME.

profiles of methanol for the Cu/SiO_2 and SiO_2 samples, however, exhibit much lower intensity. The methanol desorbed from the SiO_2 sample is presumably attributed to the methanol pre-adsorbed on the silanol groups[102]. The slightly lower intensity and broader shape of the methanol desorption profiles of the Cu/SiO_2 sample compared to that of the SiO_2 sample are likely due to the CuO nanoparticles in the Cu/SiO_2 sample covering silanol sites responsible for methanol adsorption and creating new adsorption sites on the CuO nanoparticles, respectively. The small difference between the methanol profile of the Cu/SiO_2 and SiO_2 samples, however, indicates that CuO nanoparticles does not adsorb methanol to a large extent, which is in contrast with the Cu ions/clusters in the Cu-zeolite samples.

During methanol-TPD, DME is formed at temperatures higher than 150 °C for all samples due to methanol dehydration on the acidic sites of the samples[100,103], as shown in Figure 4.3 right panel. It is evident that the zeolite samples, *i.e.* the H-ZSM-5 and H-SSZ-13 samples, exhibit DME desorption at temperatures lower than the Cu-exchanged zeolites, *i.e.* the Cu-ZSM-5 and Cu-SSZ-13 samples. On the one hand, the lower amount of DME desorbed at lower temperatures (below 200 °C) for the Cu-ZSM-5 and Cu-SSZ-13 samples compared to their parent zeolites, the H-ZSM-5 and H-SSZ-13 samples, may be due to the Cu ions possessing the Brønsted acid sites and framework defects in the Cu-ZSM-5 and Cu-SSZ-13 samples during the ion-exchange. On the other hand, dehydration of the strongly bound methanol forming DME occurs at higher temperatures for the Cu-zeolite samples, suggesting that methanol and its derivative species interact more strongly with the isolated Cu ions/clusters in the Cu-ZSM-5 and Cu-SSZ-13 sam-

ples. Additionally, considerable amount of DME forms over the Cu-zeolite samples at temperatures higher than 150 °C, suggesting that low reaction temperature is needed for selectivity towards methanol during partial oxidation of methane over Cu-zeolites. For the Cu/SiO_2 and SiO_2 samples, lower DME desorption with desorption maximum at lower temperature (around 130 °C) is observed compared to all zeolite samples. The lower amount of DME formed over the Cu/SiO_2 sample is likely due to the CuO nanoparticles covering some silanol groups on the silica surface which are responsible for DME formation. Moreover, the comparison between the DME desorption profile for Cu/SiO_2 and the Cu-zeolite samples reinforces that isolated Cu ions/clusters are responsible for the strong interaction with methanol and its derivative species rather than the CuO particles.

Evolution of surface species

As methanol-TPD measurements in the flow reactor system reveal the interaction of methanol with Cu-zeolite by analysing desorbed gas phase species, information of the sample surface remains unknown. Therefore, the dynamic interaction of methane and its derivatives with the Cu-ZSM-5 and H-ZSM-5 samples was explored during methanol desorption using *in situ* DRIFTS. Paper III includes characterisation and the DRIFTS measurements for the Cu-ZSM-5 sample and its parent H-ZSM-5. In this section, the results in Paper III are summarised.

Paper III contains assignments for all important surface species during methanol desorption. The main objectives of Paper III are to establish a steppingstone as reference for future studies on similar systems as well as to seek reasons for necessity of methanol extraction during partial oxidation of methane to methanol. Figure 4.4 presents an example of one set of DRIFT spectra taken during methanol-TPD from the Cu-ZSM-5 sample. The C-H stretching vibration region of the spectra collected at high temperatures is highlighted. The species contributing to some of the absorption features in the highlighted region is illustrated in the right panel of Figure 4.4.

The entire methanol desorption process from the Cu-ZSM-5 and H-ZSM-5 samples can be summarised as follows. Upon introduction of methanol, weak interactions between the zeolite framework and methanol are formed, resulting in methanol related C-H stretching bands and perturbed zeolitic O-H vibrations in the DRIFT spectra of both the Cu-ZSM-5 and the H-ZSM-5 sample. Some negative peaks in the O-H stretching region of the spectra collected over the H-ZSM-5 sample are related to methanol adsorption on defects in the zeolite framework structure and acidic sites in H-ZSM-5. These peaks are absent in the spectra of the Cu-ZSM-5 sample, indicating replacement of the protons in hydroxyl groups at zeolitic defects and the Brønsted acid sites with Cu ions due to the ion-exchange. Additionally, dehydration of methanol takes place

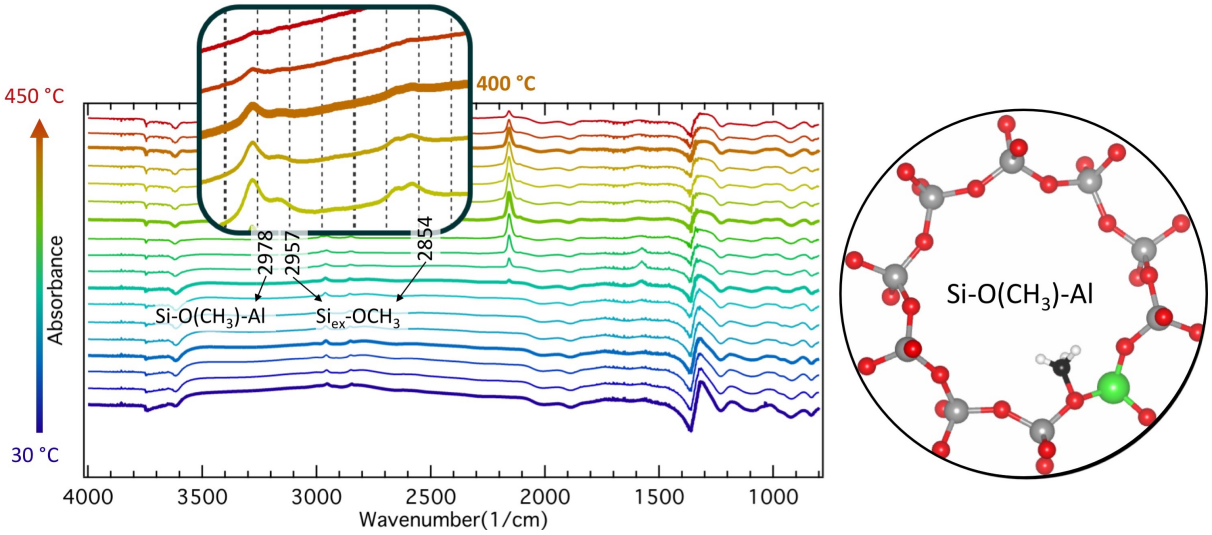

Figure 4.4: Left panel: series of selected DRIFT spectra collected during methanol-TPD from 30 to 450 °C in Ar from Cu-ZSM-5 with 24 hours ion-exchange time. The zoomed in panel is the absorption features in the C-H stretching vibration region at higher temperatures. Right panel: one of the structures related to the absorption bands at higher temperature. Atomic colours: silicon (grey), oxygen (red), aluminium (green), carbon (black), and hydrogen (white).

directly after methanol adsorption forming water on the Cu-ZSM-5 sample, generating the water deformation band in the IR spectra (1647 cm^{-1}). The absence of this band in the H-ZSM-5 sample spectra suggests that low-temperature dehydration of methanol takes place at the Cu sites. With increasing temperature, the liquid-like methanol desorbs and stronger interactions begin to form on both samples. For the H-ZSM-5 sample spectra, methoxy groups become observable on extra framework Al sites at 150 °C followed by DME formation over the Brønsted acid sites at 200 °C. Whereas for the Cu-ZSM-5 sample, due to the Cu ions at the ion-exchange sites, these bands are less evident. Formation of formate and CO, however, is evident for the Cu-ZSM-5 sample only, suggesting further oxidation of methanol and methoxy groups on the Cu sites. At temperature above 300 °C, methoxy groups bound with Brønsted acid sites and silanol groups become prominent for both samples, as shown in the highlighted part in Figure 4.4. These bands remain with decreased intensity at 450 °C indicating that methoxy groups bind strongly on the ZSM-5 framework.

The conclusions for Paper III can be summarised as follows: i) the Brønsted acid sites and defect sites in the framework structure of the zeolite, *i.e.* extra framework Al and silanol groups, constitute ion-exchange sites for Cu ions; ii) the Cu species in Cu-ZSM-5 are responsible for interaction with methanol that is additional to the methanol adsorbed on the ZSM-5 framework sites, in consistency with the methanol desorption profile shown in Figure 4.3a; iii) the Cu species in Cu-ZSM-5 are responsible for further oxidation of methanol and methoxy groups to formate and CO, resulting in higher CO and CO_2 desorption at higher temperatures; iv) strong interactions are observed be-

tween methoxy groups and some zeolitic framework sites, *i.e.* the Brønsted acid sites and silanol groups, suggesting the necessity of the proton extraction step during direct partial oxidation of methane to methanol over Cu-ZSM-5.

4.3 Tuning the acidity of zeolite framework

The IR studies shown in both Section 4.2 and 4.1 lead to the conclusion that the Brønsted acid sites in zeolites play an important role for the methanol desorption. More specifically, the strong acidity of the Brønsted acid sites may hinder methanol forming from methoxy species. Therefore, it is of great interest to investigate partial oxidation of methane to methanol over zeotypes facilitating similar Cu sites to zeolites but possessing different acidity. This is presented in the following section on Cu-boron silicate. Moreover, being able to corporate transition metals into zeolite framework structure may give the possibility to control zeotype acidity and stabilising metal sites simultaneously. This is presented in the last part of the study on Fe and/or Al silicate.

Properties of Cu-boron silicate with CHA structure

On the purpose of synthesising a material with decreased framework acidity of SSZ-13, a boron containing silicate with CHA framework structure (BS) was prepared in a direct route, as described in Paper IV. To functionalise the BS sample for oxidation of methane to methanol, Cu was ion-exchanged to the BS sample using aqueous ion-exchange.

As shown in Figure 4.5a and b, the morphology of the BS crystal is presented to be rhombohedtral and almost cubic shaped which is typical for the CHA framework

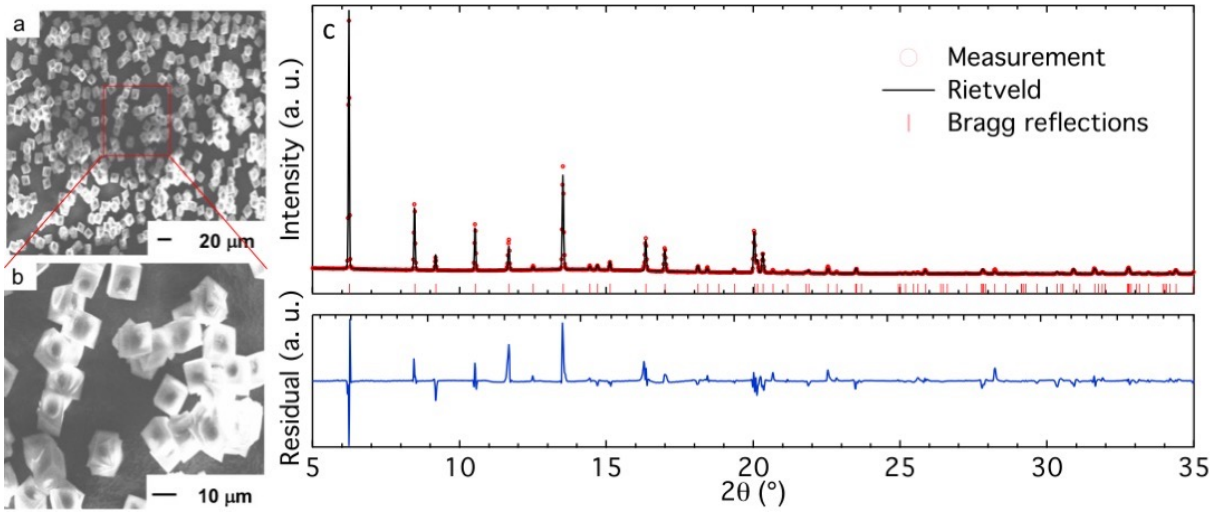

Figure 4.5: (a, b) SEM images of the BS sample. (c) High-resolution X-ray diffractogram and Rietveld refinement of the BS sample.

Table 4.1: The BET surface area (S_{BET}), micropore volume ($V_{micropore}$) and average heat of NH_3 adsorption (ΔH) for the BS, Cu-BS, H-SSZ-13 and Cu-SSZ-13 sample.

	BS	Cu-BS	H-SSZ-13	Cu-SSZ-13
S_{BET} (m^2g^{-1})	533	499	657	632
$V_{micropore}$ (cm^3g^{-1})	0.24	0.23	0.26	0.23
ΔH (kJ/mol)	-41.2	-88.2	-110	-132

structure.[104] The high-resolution X-ray diffractogram in Figure 4.5c presents reflections characteristic for the CHA framework structure. No extra reflections can be observed from the XRD pattern indicating the incorporation of boron and silicon into the framework positions.

The surface area (S_{BET}), micropore volume ($V_{micropore}$) and average heat of NH_3 adsorption (ΔH) of the synthesised BS and Cu-BS samples were evaluated together with the reference samples (H-SSZ-13 and Cu-SSZ-13) using N_2 sorption and NH_3 adsorption. The values are summarised in Table 4.1. The values of S_{BET} and $V_{micropore}$ of the BS sample are lower than those of the aluminium-containing counterparts, the H-SSZ-13 sample, which is in line with previous study on boron containing zeotypes[105]. The values of S_{BET} and $V_{micropore}$ are lower for the Cu-BS sample compared to the parent BS sample, which is in trend with the Cu-SSZ-13 and H-SSZ-13 sample. This is reasonable as Cu atoms occupy space in the chabazite cages that the space for N_2 is limited. The N_2 sorption results indicate that no detrimental change is observed after Cu ion-exchange to the BS sample. The acidity of the material can be reflected by the heat of ammonia adsorption, ΔH. The heat of adsorption for the BS sample (-41.2 kJ/mol) compared with that for the H-SSZ-13 sample (-110 kJ/mol) is much lower in absolute value, indicating a considerably lower acidity of the BS sample. Introducing Cu to the BS sample, however, results in an increase in the absolute value of ΔH (-88.2 kJ/mol), suggesting a higher acidity of the Cu sites in the Cu-BS sample. Such acidity increase is also obvious for the Cu-SSZ-13 sample (-132 kJ/mol) compared with its parent H-SSZ-13 sample.

To investigate the interaction between methanol and the synthesised BS and Cu-BS samples, methanol-TPD experiments were carried out on these two samples along with the reference H-SSZ-13 sample. The recorded spectra are presented in Figure 4.6. For the H-SSZ-13 sample, as shown in Figure 4.6a, methanol is hydrogen-bonded to the sample (2954 and 2847 cm^{-1})[76,100,106] at temperatures below 150 °C. With temperature increase, these pre-adsorbed methanol starts to interact with the Brønsted acid sites (2834 cm^{-1}) and is converted to methoxy species (2979 cm^{-1}).[76] The formed methoxy species remain on the Brønsted acid sites (2979 cm^{-1}) and the extra framework Si (2959 and 2856 cm^{-1})[65,71,76] in the H-SSZ-13 sample with the temperature increase to 450 °C. For the BS and Cu-BS samples, as shown in Figure 4.6b and c, the positions of the absorption bands appear to be identical. Methanol adsorption on these two samples at

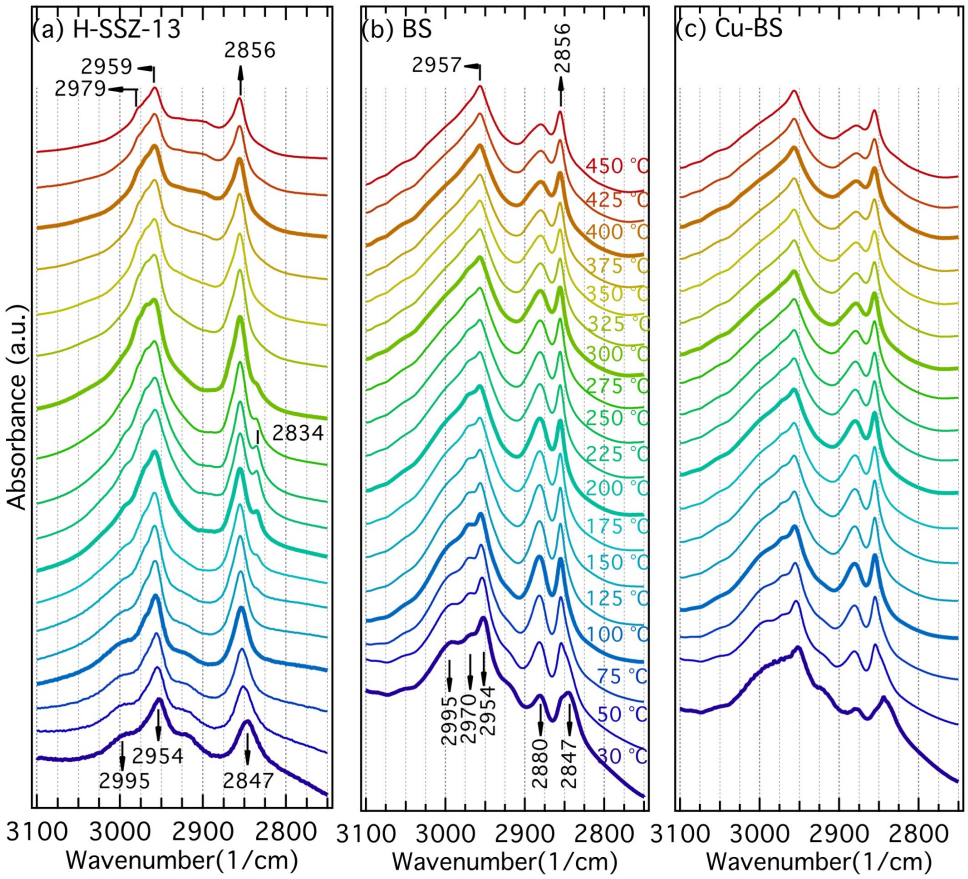

Figure 4.6: IR spectra collected for the H-SSZ-13 (a), BS (b) and Cu-BS (c) samples during methanol desorption from 30 to 450 °C.

25 °C appears in forms of hydrogen bonded methanol (2954 and 2847 cm^{-1})[76,100,106] and methanol adsorbed on the boron sites (2995, 2970 and 2880 cm^{-1})[107,108]. Upon temperature increase for both samples, besides speculated conversion of methanol to methoxy over the extra framework silicon sites (the blueshift of the bands at 2954 and 2847 cm^{-1} to 2957 and 2856 cm^{-1}), no obvious deprotonation of methanol can be observed over the boron sites as the boron related absorption bands remain at the same wavenumbers. This can be explained by the weaker acidity, therefore weaker ability of the boron sites to deprotonate methanol compared to the aluminium sites.

In summary, boron silicate with CHA framework structure and lower acidity compared to the H-SSZ-13 sample was successfully synthesised. A Cu-boron silicate was obtained by ion-exchange of the BS sample in a Cu containing solution. No obvious damage to the BS pore structure is observed after ion-exchange, while the acidity is increased due to the introduction of the Cu sites. Methanol-TPD experiments exhibit no obvious deprotonation of the methanol over the boron sites for both the BS and Cu-BS sample, which is in contrary to the methoxy formation over the aluminium sites in the H-SSZ-13 sample. These properties of the Cu-BS sample makes it a promising catalyst

for partial oxidation of methane to methanol without the extraction step.

Methane oxidation over the Cu-boron silicate

To further explore the possibility of the Cu-BS sample as a catalyst for methane to methanol, an IR study of methane oxidation was carried out over the pre-oxidised and pre-reduced sample, as shown in Figure 4.7. The formation of methoxy species over the Cu sites (2924 and 2855 cm^{-1}) [109–112] exclusively over the pre-oxidised Cu-BS sample but not the pre-reduced sample indicates the possibility of the Cu sites in the Cu-BS sample to form Cu species active for methane activation when activated under oxidising condition. Unlike its Al containing counterpart Cu-SSZ-13 (see Figure 4.2), where the methoxy species are observed on the zeolite framework and defects rather than the Cu sites during methane oxidation, no methoxy species on boron or silicon sites can be observed for the Cu-BS sample. This can be explained by the weaker acidity of the boron sites compared to the aluminium sites.

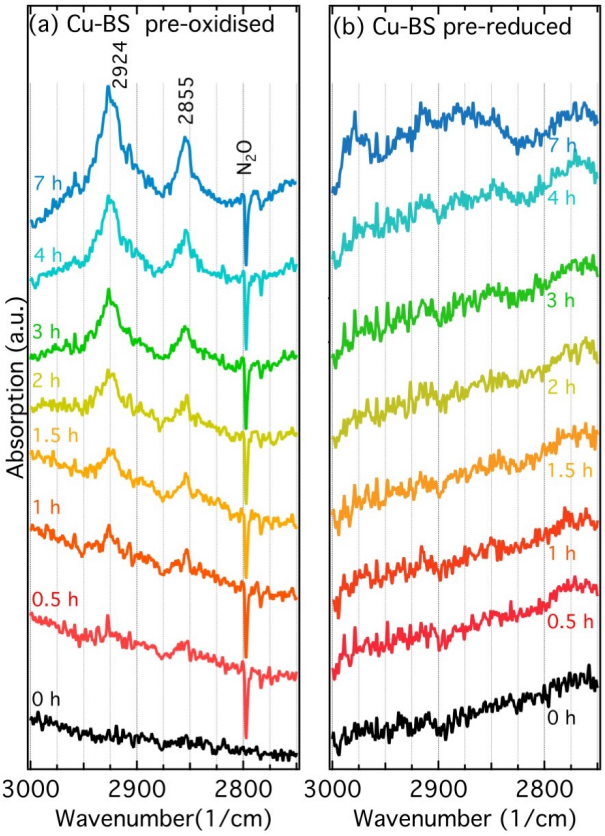

Figure 4.7: IR spectra for the pre-oxidised (a) and pre-reduced (b) Cu-BS sample under exposure of methane at 250 °C for 0 to 7 h.

Properties of Fe and/or Al containing silicate with MFI structure

Four samples with MFI framework structure were synthesised for this part of the study: silicate (S), Fe containing silicate (FS), Al containing silicate (AS) as well as Fe and Al containing silicate (FAS). The goal was to tune the framework acidity by incorporating Fe and/or Al into the framework structure. The MFI crystalline structures of all samples were confirmed by XRD measurements. The BET surface area and the micropore volume of of all samples are reasonable for materials with MFI framework structure, see Paper V. The FS, AS and FAS samples were ion-exchanged to their NH_4^+ form and subsequently calcined to the H^+ form: H-FS, H-AS and H-FAS.

The acidity of the zeotypes/zeolite can be reflected by the absorption wavenumber

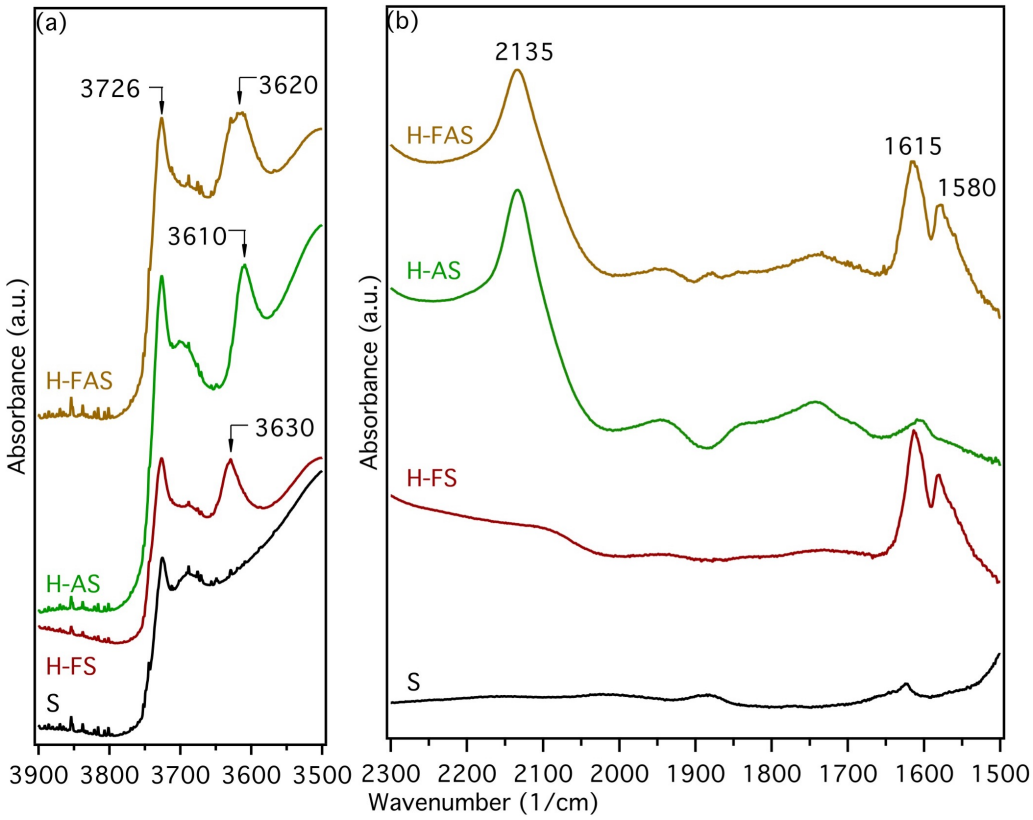

Figure 4.8: IR spectra of the calcined (a) and NO exposed (b) S, H-FS, H-AS and H-FAS sample.

of the OH groups in their IR spectrum. The OH stretching vibration region of the IR spectra collected from the S, H-FS, H-AS and H-FAS samples is presented in Figure 4.8a. The spectra from all samples present a peak centred at 3726 cm^{-1} which originates from silanol groups at zeolite boundary or defects[65,67,71,76,100,106,113,114]. Additional peaks at 3630, 3610 and 3620 cm^{-1} can be observed for the H-FS, H-AS and H-FAS sample, respectively. These bands are presumably assigned to the OH stretching vibrations in the Brønsted acid sites related to the framework Fe and/or Al. According to a previous first-principles calculation study, OH groups possessing higher acidity exhibit absorption bands at lower wavenumbers[115]. Therefore, it is reasonable to conclude that the acidity of the four samples are as follow: S<H-FS<H-AS<H-FAS.

NO adsorption was carried out to probe metal species in the S, H-FS, H-AS and H-FAS samples. The IR spectra recorded after NO exposure are presented in Figure 4.8b. An absorption band at 2135 cm^{-1} rises upon NO exposure for the Al containing samples, *i.e.* the H-AS and H-FAS samples. This band is associated with NO^{+} at cation position[116], presumably beside Al, in the microporous structure. Moreover, absorption bands at 1615 and 1580 cm^{-1} are evident for the Fe containing samples, *i.e.* the H-FS and H-FAS sample. These bands are assigned to bridging and bidentate nitrates, respectively[117]. The formation of nitrate indicates that the Fe species in the Fe containing samples are

able to oxidise NO. Though it is clear that such Fe species are not in form of Fe ions in the ion-exchange positions[116] or larger Fe species (oxides, particles or oligomers)[118–121], the nature of these Fe species remains unclear. The oxidising property of such Fe species, however, may be interesting for methane activation.

4.4 Some reflections on methodological approaches

To progress the understanding of metal-exchanged zeolites/zeotypes and the catalytic processes behind partial oxidation of methane to methanol over these materials, hitherto a reaction showing notably low methanol production, strong requirements are put on scientific methods and laboratory instrumentation. The corresponding discussion in the scientific literature on methane to methanol conversion, however, seems considerably underestimated.

Conducting kinetic analysis, i.e., measuring the activity/selectivity of the catalysts in chemical reactors, the low methanol production stretches the need for lower detection limits of most experimental set-ups by bringing difficulties in both reactor design and analysis methods for detection. To measure relevantly low concentrations of methanol, gas chromotography (GC) was first used for batch mode reaction where all methanol produced over Cu-zeolites during one quasi-catalytic cycle was extracted and quantified.[32,33,35,47,52,55,73] Later on, mass spectrometry (MS)[38,43,48,49,57,122] or GC[50,53,54,95] were introduced for downstream analysis of methanol during the extraction step of the quasi-catalytic cycle as well as during catalytic methane conversion. The flow reactors used in these studies are designed for powder or pellet samples and the amount of sample used ranges from 0.1 to 2 g. Those reactors may suffer from high pressure drop and uneven temperature distribution within the sample bed when high gas flow rates are used and/or if the reactor design is flawed[123]. Although not ideal for reactions that may need considerable residence time to produce product concentrations of the order of ppm, the monolith flow reactor used in this study (see Section 3.2), however, provides reaction conditions that allows for good control of temperature profile[123] and facilitates analysis methods that requires high gas velocity.

For observation of active sites and reaction mechanism of methane to methanol, various *in situ/operando* techniques have previously been used, *e.g.* Raman spectroscopy, UV-vis spectroscopy, XAS and IR spectroscopy. For identification of the active site structure, it is necessary to combine Raman spectroscopy or UV-vis spectroscopy with first-principles calculations. Though these type of calculations gives precise structure of energetically plausible sites and their predicted vibrational resonance frequencies, the interpretation of UV-vis spectra can be vague due to broad absorption bands at this region. While for mechanism study, though both XAS and IR spectroscopy can give

information under realistic reaction conditions, they have their own limitations. XAS gives an average configuration of the element under interest, which is not active site sensitive. IR spectroscopy captures stable reaction intermediates, which may result in missing information of the unstable species during the reaction. Moreover, assignment of the absorption features often requires many reference spectra either from known literature or experiments carried out parallely to the study if not both.

CHAPTER 5
CONCLUSIONS AND OUTLOOK

5.1 Concluding remarks

Summarising, this thesis treats partial oxidation of methane over copper zeolites and Cu/SiO_2, methanol desorption from copper functionalised zeolites and zeotypes, as well as tuning the acidity of zeotypes. For partial oxidation of methane to methanol, copper ion-exchanged zeolites and Cu/SiO_2 were characterised and tested for their activity towards methanol formation. The characterisation of the materials concluded that the majority of the copper species in the copper zeolite samples are copper cations/cluster while the Cu/SiO_2 sample consists mainly of copper nanoparticles. The results of the activity tests suggest that copper cations/clusters in the copper zeolite samples are responsible for methanol formation. Interestingly, small amounts of methanol are produced over the Cu/SiO_2 sample, suggesting higher flexibility in support material for copper species active for partial oxidation of methane to methanol. Moreover, IR studies of all samples suggest conversion of methane to methoxy species adsorbed on non-copper sites during the reaction step of the quasi-catalytic cycle. The desorption of methoxy species from the copper zeolite samples during the extraction step indicates methanol formation from methoxy and water.

To understand the necessity of the extraction step of the quasi-catalytic cycle, methanol-TPD experiments were carried out over the copper exchanged zeolites. The conclusions from the flow reactor and IR study can be summarised as follows: i) isolated copper ions on ion-exchange sites in the zeolite framework structure are responsible for the stronger interactions with methanol and its derivatives during methanol-TPD; ii) the Brønsted acid sites and defects in the framework structure of the zeolite provide possible ion-exchange sites for copper ions; iii) the copper species in copper zeolite are responsible for further oxidation of methanol and methoxy groups to formate and CO,

resulting in the CO and CO_2 desorption at higher temperature; iv) strong interactions are formed between methoxy groups and some zeolitic framework sites, suggesting the necessity of the proton extraction step during direct partial oxidation of methane to methanol over zeolite containing materials.

With the understanding from the methanol-TPD study, attempts were made to tune the acidity of the zeolite framework structure for exploring the possibility of reducing the interaction between framework and methoxy species. For this purpose, five zeolites and zeotypes were synthesised. In one study, a boron silicate with chabazite framework structure was successfully synthesised. The acidity of the boron silicate and the copper boron silicate samples is lower than that of their zeolite counterparts, *i.e.*, the H-SSZ-13 and Cu-SSZ-13, respectively. During methanol-TPD experiments from 30 to 450 °C, methanol does not deprotonate over the boron silicate and copper boron silicate samples, suggesting that the copper boron silicate sample is a promising candidate for avoiding water extraction during partial oxidation of methane to methanol. Moreover, the methane oxidation experiment showed that the copper species in the oxidised copper boron silicate sample are capable of dissociating methane and the formed methoxy groups stay on the copper sites with prolonged reaction time. In the other study, three zeotypes and one zeolite with MFI structure were successfully synthesised: silicate, iron silicate, aluminum silicate and iron-aluminum silicate. The IR study showed that these zeotypes/zeolites exhibit different acidity with the following order: silicate < iron silicate < iron-aluminum silicate < aluminum silicate. Moreover, the iron species in the iron containing silicates exhibit oxidising property during NO adsorption experiments.

5.2 Outlook

For partial oxidation of methane to methanol, methane dissociation and selectivity towards methanol favours contradictory properties of the catalytic material. Based on our current knowledge, both active sites and support materials play important roles in this reaction. Controlled manufacturing of zeolites with certain Al distributions may provide possible ion-exchange sites that leads to increased amount of certain copper centres. For instance, zeolites with high amount of aluminum pairs resulting in higher percentage of copper dimers or trimers[36]. Being able to tune the distribution of various copper species, one could study the correlation between methanol productivity and different copper species.

As zeolite structures stabilise the methoxy groups and prevent them from further oxidation[77,124], it is also difficult to obtain the final product methanol. Proton extraction is necessary according to our work, and the proton sources we are using now are water or other organic compounds with easily dissociated protons. This extraction pro-

cess may in turn bring in unwanted hydroxyl groups, blocking the copper centres, and therefore terminating the reaction. To avoid blockage of active sites, it may be reasonable to find a proton source that does not introduce other unwanted species. Moreover, our studies show that it is possible to tune the acidity of zeotypes, which in turn can influence the interaction between methanol and framework structure. Copper containing boron silicate has shown promise and can be tested for the quasi-catalytic or even catalytic cycle of partial oxidation of methane to methanol.

Though there is no consensus of the active copper sites for methane to methanol in various zeolite systems and the activity is most likely related to many different copper species, one common feature of these copper species is that they are well dispersed in forms of monomer, dimer, trimer or oligomers. Moreover, previous studies and our work show that silica supported copper is active for partial oxidation of methane to methanol suggesting the possibility of support materials other than zeolites to host such dispersed copper ions and clusters. Given this, a screening of copper supported on various materials, *e.g.* alumina, silica and modified zeolites with different pore size and structure, may provide information of the requirements for forming the active copper species.

Acknowledgements

The research presented in this thesis was carried out at the Division of Applied Chemistry and the Competence Centre for Catalysis (KCK) at the Department of Chemistry and Chemical Engineering at Chalmers University of Technology, Göteborg, Sweden, during the period of August 2014 to November 2018.

This work is financially supported by the Swedish Research Council through the Röntgen-Ångström collaborations "Catalysis on the atomic scale" (No. 349-2011-6491) and "Time-resolved in situ methods for design of catalytic sites within sustainable chemistry" (No. 349-2013-567), and the Swedish Energy Agency through the FFI program “Fundamental studies on the influence of water on oxidation catalyst for biogas applications” (No. 40274-1).

The Competence Centre for Catalysis is hosted by Chalmers University of Technology and financially supported by Chalmers University of Technology, the Swedish Energy Agency and the member companies: AB Volvo, ECAPS AB, Johnson Matthey AB, Preem AB, Scania CV AB, Umicore Denmark ApS and Volvo Car Corporation AB.

Part of the research has been carried out at MAX IV Laboratory (Lund, Sweden). I would like to thank beamline I811 (MAX IV Laboratory) for providing the beamtime and the beamline staffs for their assistance.

This thesis is made possible with efforts from many individuals:

My main supervisor Per-Anders Carlsson, thank you for your understanding, support and guidance through these years. You made this somewhat painful learning process more cheering. You always have my back when it gets tough. I particularly appreciate the discussions both about science and about the experience as a scientist. Also, your patience and availability is very important for my growth during the PhD study.

My co-supervisors, Magnus Skoglundh and Anders Hellman, thank you for your discussion and input. It is nice to always have support from you on writing and when the challenge gets too physical.

Ann Jokobsson and Frida Andersson, thank you for fulfilling all my tedious requests. The division cannot function without you.

My theoretician Adam Arvidsson, you are an inspiring person. Thank you for making physics appear easier to me. I appreciate all the questions and discussion.

Hanna Härelind, thank you for your encouragement on my work and my Swedish. I appreciate your straightforwardness. Henrik Grönbeck, thank you for the attention, and

very thought through questions and discussions at the KCK meetings and KAW meetings. Louise Olsson, thank you for the help with the caloriemeter at the very stressful moment of my study.

My collaborators Johan Gustafson and Chu Zhang, than you for the discussions and suggestions at the project meetings, as well as your kind guidance during the time at PETRA III and MAX IV Laboratory.

Lasse, Lennart and Ulf, thank you for all the help in the reactor labs.

Besides the scientific/administrative support, this journey is not complete without my colleagues and friends:

My fellow colleagues of KCK and TYK, current or past, thank you for the fun we had together. I appreciate your company for all the conferences we joined, hikes we went, port wines and beers we drank, sports we participated, games we played, sauna we enjoyed, life we discussed and of course the "fika" we took. I would like to thank (alphabetic order): Alvaro, Anand, Andreas S., Andy, Anna M., Anne W., Astrid, Carl-Robert, Chris, Felix, Giulio, Gunnar, Hanzhu, Joakim, Johan N., Johanna E., Lidija, Lin C., Linda, Marika, Mats, Maxime, Mikael, Nadya, Natalia, Peter, Romain, Ron, Saba, Sam, Shishkin, Simon I., Simone, Unni and Yifei.

Special thanks go to:
Anna Pekkari and Caroline, thank you for being there for me when I am stressed and listening to my complaints. Milene and Adriano, thank you for making it feel like home in Gothenburg. Ida, Maria, Fredrik, Rikard, Mikkel and Caroline, thank you for the fun we had playing music and drinking beer together. Daniel L., Anna-Karin S., Melanie and Serusa, thank you for all the time we spent together. You made the winter here cosy and warm. I am very lucky having you as my partner and friends. Thank you all for your openness, patience and of course the fun together!

Last but not the least, my parents, for your support, understanding and encouragements.

Xueting Wang
Göteborg, October 2018

BIBLIOGRAPHY

[1] *International Association for Natural Gas Vehicles*, Retrieved 2017-04-18, **http://www.iangv.org/current-ngv-stats/**.

[2] N. A. of Engineering, *Frontiers of Engineering: Reports on Leading-Edge Engineering from the 2014 Symposium*, The National Academies Press, 107-116, 2015.

[3] *Opinion of the EEA Scientific Committee on Greenhouse Gas Accounting in Relation to Bioenergy*, EEA Scientific Committee, 2011.

[4] *Gas South Compressed Natural Gas*, Retrieved 2017-04-18, **https://www.gas-south.com/business/compressed-natural-gas.aspx**.

[5] V. Ramaswamy, O. Boucher, J. Haigh, D. Hauglustaine, J. Haywood, G. Myhre, T. Nakajima, G. Shi, and S. Solomon, *Intergovernmental Panel on Climate Change*, 2001, **Ch. 6.12**, 385.

[6] M. Soltanieh, A. Zohrabian, M. J. Gholipour, and E. Kalnay, *Int. J. Greenhouse Gas Control*, 2016, **49**, 488 – 509.

[7] Z. Zakaria and S. Kamarudin, *Renewable Sustainable Energy Rev.*, 2016, **65**, 250–261.

[8] M. J. da Silva, *Fuel Process. Technol.*, 2016, **145**, 42–61.

[9] H. Dai, *Sci. Bull.*, 2015, **60**(19), 1708–1710.

[10] J. Gong and R. Luque, *Chem. Soc. Rev.*, 2014, **43**, 7466–7468.

[11] J. J. Berzelius, *Royal Swedish Academy of Sciences*, 1835.

[12] E. Fulhame, *Philadelphia: Printed and sold by James Humphreys, corner of Second and Walnut-street*, 1810, pp. 8306–8313.

[13] A. A. Arvidsson, V. P. Zhdanov, P.-A. Carlsson, H. Grönbeck, and A. Hellman, *Catal. Sci. Technol.*, 2017, **7**, 1470–1477.

[14] Y. Ji, G. Mao, Y. Wang, and M. Bartlam, *Front. Microbiol.*, 2013, **4**, 58.

[15] C. Citek, J. B. Gary, E. C. Wasinger, and T. D. Stack, *J. Am. Chem.l Soc.*, 2015, **137**(22), 6991–4.

[16] *Protein Data Bank in Europe*, 2014, **http://www.ebi.ac.uk/pdbe/entry/pdb/4pi2**.

[17] A. R. Kulkarni, Z.-J. Zhao, S. Siahrostami, J. K. Nørskov, and F. Studt, *Catal. Sci. Technol.*, 2018, **8**, 114–123.

[18] M. Ravi, M. Ranocchiari, and J. A. van Bokhoven, *Angew. Chem. Int. Ed.*, 2017, **56**(52),

16464–16483.
[19] T. Ikuno, J. Zheng, A. Vjunov, M. Sanchez-Sanchez, M. A. Ortuño, D. R. Pahls, J. L. Fulton, D. M. Camaioni, Z. Li, D. Ray, B. L. Mehdi, N. D. Browning, O. K. Farha, J. T. Hupp, C. J. Cramer, L. Gagliardi, and J. A. Lercher, *J. Am. Chem. Soc.*, 2017, **139**(30), 10294–10301.
[20] S. Impeng, P. Khongpracha, C. Warakulwit, B. Jansang, J. Sirijaraensre, M. Ehara, and J. Limtrakul, *RSC Adv.*, 2014, **4**(24), 12572.
[21] P. G. Lustemberg, R. M. Palomino, R. A. Gutiérrez, D. C. Grinter, M. Vorokhta, Z. Liu, P. J. Ramírez, V. Matolín, M. V. Ganduglia-Pirovano, S. D. Senanayake, and J. A. Rodriguez, *J. Am. Chem. Soc.*, 2018, **140**(24), 7681–7687.
[22] C. E. Taylor and R. P. Noceti, *Catal. Today*, 2000, **55**, 259–267.
[23] C. E. Taylor, *Catal. Today*, 2003, **84**(1-2), 9–15.
[24] Y. Hu, Y. Nagai, D. Rahmawaty, C. Wei, and M. Anpo, *Catal. Lett.*, 2008, **124**(1-2), 80–84.
[25] F. M. Aghamir, N. S. Matin, A. H. Jalili, M. H. Esfarayeni, M. A. Khodagholi, and R. Ahmadi, *Plasma Sources Sci. Technol.*, 2004, **13**(4), 707–711.
[26] A. Indarto, J.-W. Cho, H. Lee, H. K. Song, and J. Palgunadi, *J. Rare Earths*, 2006, **24**(5), 513–518.
[27] A. Indarto, *IEEE Trans. Dielectr. Electr. Insul.*, 2008, **15**(4), 1038–1043.
[28] *International Zeolite Association Webpage*, **http://europe.iza-structure.org**.
[29] T. Ennaert, J. Van Aelst, J. Dijkmans, R. De Clercq, W. Schutyser, M. Dusselier, D. Verboekend, and B. F. Sels, *Chem. Soc. Rev.*, 2016, **45**, 584–611.
[30] C.-M. Wang, R. Y. Brogaard, Z.-K. Xie, and F. Studt, *Catal. Sci. Technol.*, 2015, **5**, 2814–2820.
[31] J. S. Woertink, P. J. Smeets, M. H. Groothaert, M. A. Vance, B. F. Sels, R. A. Schoonheydt, and E. I. Solomon, *Proc. Natl. Acad. Sci.*, 2009, **106**(45), 18908–18913.
[32] M. H. Groothaert, P. J. Smeets, B. F. Sels, P. A. Jacobs, Schoonheydt, and R. A., *J. Am. Chem. Soc.*, 2005, **127**, 1394–1395.
[33] P. J. Smeets, M. H. Groothaert, and R. A. Schoonheydt, *Catal. Today*, 2005, **110**(3-4), 303–309.
[34] M. H. Sazinsky and S. J. Lippard, in *Sustaining Life on Planet Earth: Metalloenzymes Mastering Dioxygen and Other Chewy Gases*, ed. P. M. H. Kroneck and M. E. Sosa Torres, Springer International Publishing, Cham, 2015; pp. 205–256.
[35] N. V. Beznis, B. M. Weckhuysen, and J. H. Bitter, *Catal. Lett.*, 2010, **138**(1-2), 14–22.
[36] M. A. C. Markovits, A. Jentys, M. Tromp, M. Sanchez-Sanchez, and J. A. Lercher, *Top. Catal.*, 2016, **59**, 1554–1563.
[37] T. Sheppard, H. Daly, A. Goguet, and J. M. Thompson, *ChemCatChem*, 2016, **8**(3), 562–570.
[38] T. Sheppard, C. D. Hamill, A. Goguet, D. W. Rooney, and J. M. Thompson, *Chem. Commun.*, 2014, **50**(75), 11053–5.
[39] K. Narsimhan, K. Iyoki, K. Dinh, and Y. Roman-Leshkov, *ACS Cent. Sci.*, 2016, **2**(6),

424–9.
[40] S. Grundner, M. A. C. Markovits, G. Li, M. Tromp, E. A. Pidko, E. J. M. Hensen, A. Jentys, M. Sanchez-Sanchez, and J. A. Lercher, *Nat. Commun.*, 2015, **6**, 7546.
[41] A. Sainz-Vidal, J. Balmaseda, L. Lartundo-Rojas, and E. Reguera, *Microporous Mesoporous Mater.*, 2014, **185**, 113–120.
[42] E. M. C. Alayon, M. Nachtegaal, A. Bodi, M. Ranocchiari, and J. A. van Bokhoven, *Phys. Chem. Chem. Phys.*, 2015, **17**(12), 7681–7693.
[43] Y. Kim, T. Y. Kim, H. Lee, and J. Yi, *Chem. Commun.*, 2017, **53**, 4116–4119.
[44] P. Vanelderen, B. E. R. Snyder, M.-L. Tsai, R. G. Hadt, J. Vancauwenbergh, O. Coussens, R. A. Schoonheydt, B. F. Sels, and E. I. Solomon, *J. Am. Chem. Soc.*, 2015, **137**(19), 6383–6392.
[45] E. M. C. Alayon, M. Nachtegaal, A. Bodi, and J. A. van Bokhoven, *ACS Catal.*, 2014, **4**(1), 16–22.
[46] H. V. Le, S. Parishan, A. Sagaltchik, C. Göbel, C. Schlesiger, W. Malzer, A. Trunschke, R. Schomäcker, and A. Thomas, *ACS Catal.*, 2017, **7**(2), 1403–1412.
[47] P. Tomkins, A. Mansouri, S. E. Bozbag, F. Krumeich, M. B. Park, E. M. Alayon, M. Ranocchiari, and J. A. van Bokhoven, *Angew. Chem., Int. Ed.*, 2016, **55**(18), 5467–71.
[48] V. L. Sushkevich, D. Palagin, M. Ranocchiari, and J. A. van Bokhoven, *Science*, 2017, **356**(6337), 523–527.
[49] V. L. Sushkevich, D. Palagin, and J. A. van Bokhoven, *Angew. Chem. Int. Ed.*, 2018, **57**(29), 8906–8910.
[50] M. J. Wulfers, S. Teketel, B. Ipek, and R. F. Lobo, *Chem. Commun.*, 2015, **51**(21), 4447–4450.
[51] B. Ipek, M. J. Wulfers, H. Kim, F. Göltl, I. Hermans, J. P. Smith, K. S. Booksh, C. M. Brown, and R. F. Lobo, *ACS Catal.*, 2017, **7**(7), 4291–4303.
[52] M. B. Park, S. H. Ahn, A. Mansouri, M. Ranocchiari, and J. A. van Bokhoven, *ChemCatChem*, 2017, **9**(19), 3705–3713.
[53] D. K. Pappas, E. Borfecchia, M. Dyballa, I. A. Pankin, K. A. Lomachenko, A. Martini, M. Signorile, S. Teketel, B. Arstad, G. Berlier, C. Lamberti, S. Bordiga, U. Olsbye, K. P. Lillerud, S. Svelle, and P. Beato, *Journal of the American Chemical Society*, 2017, **139**(42), 14961–14975.
[54] B. Ipek and R. F. Lobo, *Chem. Commun. (Cambridge, U. K.)*, 2016, **52**(91), 13401–13404.
[55] S. E. Bozbag, P. Sot, M. Nachtegaal, M. Ranocchiari, J. A. van Bokhoven, and C. Mesters, *ACS Catal.*, 2018, **8**(7), 5721–5731.
[56] M. H. Groothaert, P. J. Smeets, B. F. Sels, P. A. Jacobs, and R. A. Schoonheydt, *J. Am. Chem. Soc.*, 2005, **127**(5), 1394–1395.
[57] H. V. Le, S. Parishan, A. Sagaltchik, H. Ahi, A. Trunschke, R. Schomäcker, and A. Thomas, *Chemistry – A European Journal*, 2018, **24**(48), 12592–12599.
[58] V. Sobolev, K. Dubkov, O. Panna, and G. Panov, *Catal. Today*, 1995, **24**, 251–252.
[59] G. Panov, V. Sobolev, K. Dubkov, V. Parmon, N. Ovanesyan, A. Shilov, and A. Shteinman,

React. Kinet. Catal. Lett., 1997, **61**(2), 251–258.
[60] K. Yoshizawa, Y. Shiota, T. Yumura, and T. Yamabe, *J. Phys. Chem.*, 2000, **104**(734-740).
[61] P. Knops-Gerrits and W. G. III, *J. Mol. Catal. A: Chem.*, 2001, **166**, 135–145.
[62] B. Michalkiewicz, *Appl. Catal., A*, 2004, **277**(1-2), 147–153.
[63] S. Pabchanda, P. Pantu, and J. Limtrakul, *J. Mol. Catal. A: Chem.*, 2005, **239**(1-2), 103–110.
[64] M. V. Parfenov, E. V. Starokon, L. V. Pirutko, and G. I. Panov, *J. Catal.*, 2014, **318**, 14–21.
[65] B. R. Wood, J. A. Reimer, A. T. Bell, M. T. Janicke, and K. C. Ott, *J. Catal.*, 2004, **225**(2), 300–306.
[66] E. V. Starokon, M. V. Parfenov, L. V. Pirutko, S. I. Abornev, and G. I. Panov, *J. Phys. Chem. C*, 2011, **115**(5), 2155–2161.
[67] E. V. Starokon, M. V. Parfenov, S. S. Arzumanov, L. V. Pirutko, A. G. Stepanov, and G. I. Panov, *J. Catal.*, 2013, **300**, 47–54.
[68] B. E. R. Snyder, P. Vanelderen, M. L. Bols, S. D. Hallaert, L. H. Böttger, L. Ungur, K. Pierloot, R. A. Schoonheydt, B. F. Sels, and E. I. Solomon, *Nature*, 2016, **536**, 317.
[69] N. V. Beznis, B. M. Weckhuysen, and J. H. Bitter, *Catal. Lett.*, 2009, **136**(1-2), 52–56.
[70] N. V. Beznis, A. N. C. van Laak, B. M. Weckhuysen, and J. H. Bitter, *Microporous Mesoporous Mater.*, 2011, **138**(1-3), 176–183.
[71] M. C. Kung, S. S. Y. Lin, and H. H. Kung, *Top. Catal.*, 2012, **55**(1-2), 108–115.
[72] Y. K. Krisnandi, B. A. P. Putra, M. Bahtiar, Zahara, I. Abdullah, and R. F. Howe, *Procedia Chem.*, 2015, **14**, 508–515.
[73] P. Tomkins, M. Ranocchiari, and J. A. van Bokhoven, *Acc. Chem. Res.*, 2017, **50**(2), 418–425.
[74] P. Tang, Q. Zhu, Z. Wu, and D. Ma, *Energy Environ. Sci.*, 2014, **7**(8), 2580.
[75] K. Narsimhan, V. K. Michaelis, G. Mathies, W. R. Gunther, R. G. Griffin, and Y. Román-Leshkov, *J. Am. Chem. Soc.*, 2015, **137**(5), 1825–1832.
[76] X. Wang, A. A. Arvidsson, M. O. Cichocka, X. Zou, N. M. Martin, J. Nilsson, S. Carlson, J. Gustafson, M. Skoglundh, A. Hellman, and P.-A. Carlsson, *J. Phys. Chem. C*, 2017, **121**(49), 27389–27398.
[77] V. L. Sushkevich and J. A. van Bokhoven, *Catal. Sci. Technol.*, 2018, **8**, 4141–4150.
[78] P. Velin, U. Stenman, M. Skoglundh, and P.-A. Carlsson, *Rev. Sci. Instrum.*, 2017, **88**, 115102.
[79] C. Kalamaras, D. Palomas, R. Bos, A. Horton, M. Crimmin, and K. Hellgardt, *Catal. Lett.*, 2016, **146**(2), 483–492.
[80] A. de Jong and J. Niemantsverdriet, *Surf. Sci.*, 1990, **233**(3), 355 – 365.
[81] D. A. King, *Surf. Sci.*, 1975, **47**(1), 384 – 402.
[82] E. Habenschaden and J. Küppers, *Surf. Sci.*, 1984, **138**(1), L147 – L150.
[83] P. Redhead, *Vacuum*, 1962, **12**(4), 203 – 211.
[84] J. Falconer and R. Madix, *Surf. Sci.*, 1975, **48**(2), 393 – 405.
[85] W. L. Bragg, *Proc. R. Soc. London, Ser. A*, 1913, **89**(610), 248–277.
[86] P. Scherrer, *Nachr. Ges. Wiss. Goettingen, Math.-Phys. Kl.*, 1918, pp. 98–100.

[87] S. Brunauer, P. H. Emmett, and E. Teller, *J. Am. Chem. Soc.*, 1938, **60**, 309–319.
[88] C. Lamberti, S. Bordiga, M. Salvalaggio, G. Spoto, and A. Zecchina, *J. phys. Chem. B*, 1997, **101**(3), 344–360.
[89] M. H. Groothaert, J. A. v. Bokhoven, A. A. Battiston, B. M. Weckhuysen, and R. A. Schoonheydt, *J. Am. Chem. Soc.*, 2002, **125**, 7629–7640.
[90] P. Vanelderen, R. G. Hadt, P. J. Smeets, E. I. Solomon, R. A. Schoonheydt, and B. F. Sels, *J. Catal.*, 2011, **284**(2), 157–164.
[91] M.-L. Tsai, R. G. Hadt, P. Vanelderen, B. F. Sels, R. A. Schoonheydt, and E. I. Solomon, *J. Am. Chem. Soc.*, 2014, **136**(9), 3522–3529.
[92] T. Yumura, Y. Hirose, T. Wakasugi, Y. Kuroda, and H. Kobayashi, *ACS Catal.*, 2016, **6**(4), 2487–2495.
[93] G. Li, P. Vassilev, M. Sanchez-Sanchez, J. A. Lercher, E. J. M. Hensen, and E. A. Pidko, *J. Catal.*, 2016, **338**, 305–312.
[94] A. R. Kulkarni, Z.-J. Zhao, S. Siahrostami, J. K. Nørskov, and F. Studt, *ACS Catal.*, 2016, pp. 6531–6536.
[95] R. Oord, J. E. Schmidt, and B. M. Weckhuysen, *Catal. Sci. Technol.*, 2018, **8**, 1028–1038.
[96] L. Chen, L. Lin, Z. Xu, T. Zhang, D. Liang, Q. Xin, and P. Ying, Sep , 1995, **35**(3), 245–258.
[97] V. B. Kazansky, *Kinet. Catal.*, 2014, **55**(6), 737–747.
[98] V. Kazanskii, A. Serykh, and A. Bell, *Kinet. Catal.*, 2002, **43**(3), 419–426.
[99] D. G. Permenov and V. A. Radzig, *Kinet. Catal.*, 2004, **45**(1), 14–23.
[100] S. M. Campbell, X.-Z. Jiang, and R. F. Howe, *Microporous Mesoporous Mater.*, 1999, **29**, 91–108.
[101] K. I. Hadjiivanov, M. M. Kantcheva, and D. G. Klissurski, *J. Chem. Soc., Faraday Trans.*, 1996, **92**(22), 4595–4600.
[102] A. G. Pelmenschikov, G. Morosi, A. Gamba, A. Zecchina, S. Bordiga, and E. A. Paukshtis, *J. Phys. Chem.*, 1993, **97**(46), 11979–11986.
[103] P. J. Smeets, J. S. Woertink, B. F. Sels, E. I. Solomon, Schoonheydt, and R. A., *Inorg. Chem.*, 2010, **49**(8), 3573–3583.
[104] *International Zeolite Association Webpage*, **http://www.iza-online.org/natural/Datasheets/Chabazite/Chabazite.html**.
[105] J. Liang, J. Su, Y. Wang, Z. Lin, W. Mu, H. Zheng, R. Zou, F. Liao, and J. Lin, *Microporous Mesoporous Mater.*, 2014, **194**, 97–105.
[106] T. Nobukawa, M. Yoshida, S. Kameoka, S.-i. Ito, K. Tomishige, and K. Kunimori, *J. Phys. Chem. B*, 2004, **108**(13), 4071–4079.
[107] L. Regli, C. Lamberti, C. Busco, A. Zecchina, C. Prestipino, K. P. Lillerud, S. I. Zones, and S. Bordiga In ed. Xu, R and Gao, Z and Chen, J and Yan, W, *Proc. Int. Zeolite Conf., 15th*, Vol. 170 of *Studies in Surface Science and Catalysis*, pp. 585–593, 2007.
[108] L. Regli, S. Bordiga, C. Lamberti, K. P. Lillerud, S. I. Zones, and A. Zecchina, *J. Phys. Chem. C*, 2007, **111**(7), 2992–2999.
[109] M. D. Driessen and V. H. Grassian, *J. Phys. Chem.*, 1995, **99**(45), 16519–16522.

[110] M. A. Chesters and E. M. McCash, *J. Electron Spectrosc. Relat. Phenom.*, 1987, **44**, 99–108.
[111] R. Burch, S. Chalker, and J. Pritchard, *J. Chem. Soc., Faraday Trans.*, 1991, **87**(11), 1791–1794.
[112] M. P. Andersson, P. Uvdal, and A. D. MacKerell, *J. Phys. Chem. B*, 2002, **106**(20), 5200–5211.
[113] J. Sárkány, *Phys. Chem. Chem. Phys.*, 1999, **1**, 5251–5257.
[114] A. B. Ene, T. Archipov, and E. Roduner, *J. Phys. Chem. C*, 2010, **114**, 14571–14578.
[115] E. L. Meijer, R. A. van Santen, and A. P. J. Jansen, *J. Phys. Chem.*, 1996, **100**(22), 9282–9291.
[116] S. Shwan, E. C. Adams, J. Jansson, and M. Skoglundh, *Catal. Lett.*, 2013, **143**(1), 43–48.
[117] K. Hadjiivanov, H. Knözinger, B. Tsyntsarski, and L. Dimitrov, *Catal. Lett.*, 1999, **62**(1), 35–40.
[118] S. M. Park, G. Seo, Y. S. Yoo, and H.-S. Han, *Korean J. Chem. Eng.*, 2010, **27**(6), 1738–1743.
[119] M. Iwasaki, K. Yamazaki, K. Banno, and H. Shinjoh, *J. Catal.*, 2008, **260**(2), 205 – 216.
[120] G. Grubert, M. J. Hudson, R. W. Joyner, and M. Stockenhuber, *J. Catal.*, 2000, **196**(1), 126 – 133.
[121] G. Mul, J. Pérez-Ramírez, F. Kapteijn, and J. Moulijn, *Catal. Lett.*, 2002, **80**(3), 129–138.
[122] M. Dyballa, D. K. Pappas, E. Borfecchia, P. Beato, U. Olsbye, K. P. Lillerud, B. Arstad, and S. Svelle, *Microporous and Mesoporous Mater.*, 2018, **265**, 112 – 122.
[123] A. Cybulski and J. A. Moulijn, *Catal. Rev.*, 1994, **36**(2), 179–270.
[124] K. T. Dinh, M. M. Sullivan, P. Serna, R. J. Meyer, M. Dincă, and Y. Román-Leshkov, *ACS Catal.*, 2018, **8**(9), 8306–8313.